Airborne Sounding Radar for Desert Subsurface Exploration of Aquifers: Desert-SEA

Mission concept study

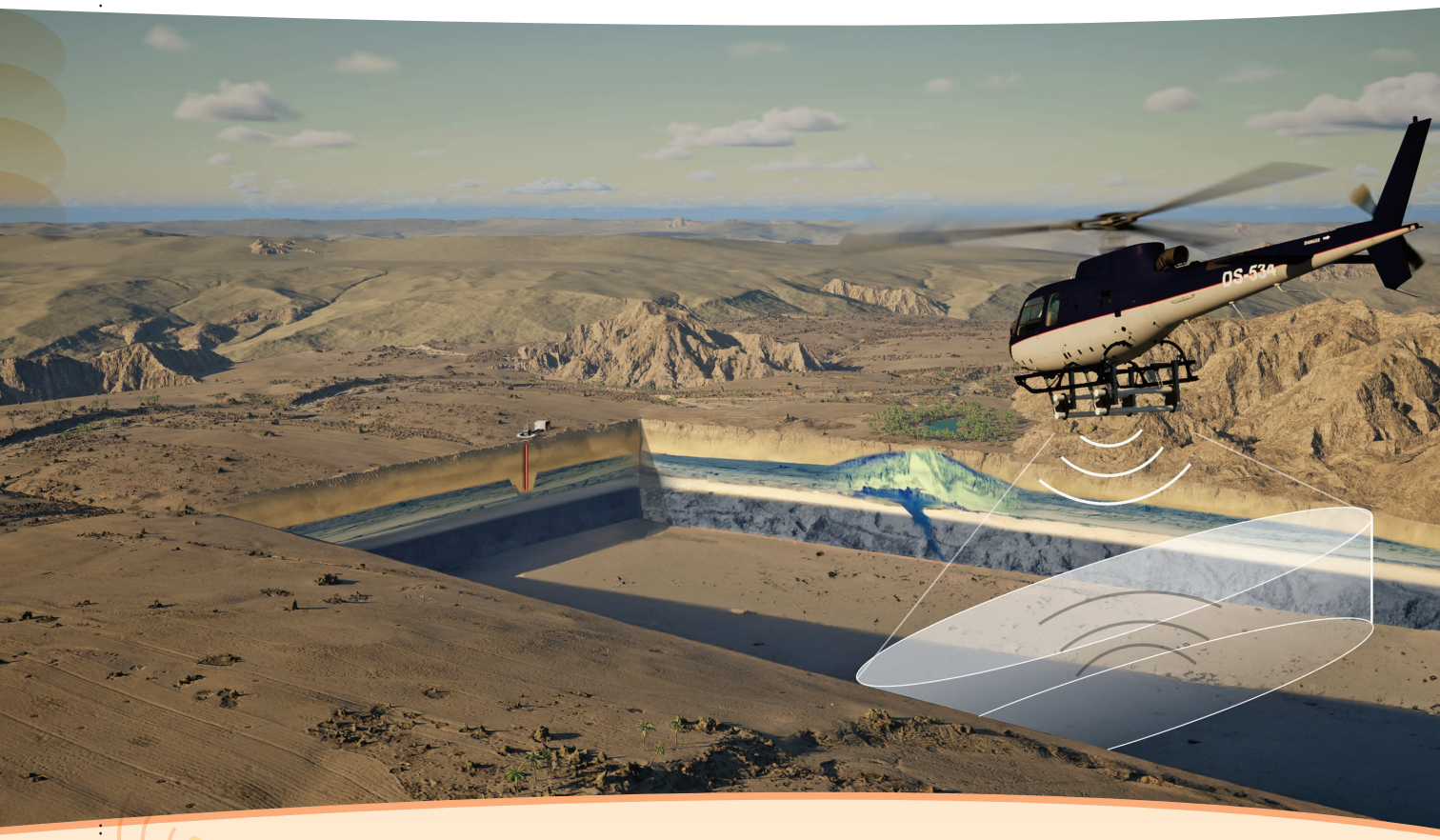

ESSAM HEGGY, MAHTA MOGHADDAM, ELIZABETH M. PALMER, WILLIAM M. BROWN, J. LEE BLANTON, MIKOŁAJ KOSINSKI, PAUL SIRRI, EDGAR A. DIXON, ABOTALIB Z. ABOTALIB, JONATHAN C. L. NORMAND, JOHN CLARK, GARY KLEMENS, MATTHIEU AGRANIER, FRANÇOIS GUILLON, AKRAM A. ABDELLATIF, TAMER KHATTAB, ZLATAN TSVETANOV, MOHAMED SHOKRY, NOOR AL-MULLA, MOHAMED RAMAH, SAYED M. BATENI, ALIREZA TABATABAEENEJAD, AND JEAN-PHILIPPE AVOUAC

Shallow aquifers are the largest freshwater bodies in the North African Sahara and the Arabian Peninsula. Their groundwater dynamics and response to climatic variability and anthropogenic discharge remain largely unquantified due to the absence of large-scale monitoring methods. Currently, the assessment of groundwater dynamics in these aquifer systems is made primarily from sporadic well logs that barely cover a few percent of the geographical extent of these water bodies. To address this deficiency, we develop the use of an ultrawideband (UWB) very high frequency (VHF) interferometric airborne sounding radar, under a collaboration between NASA and the Qatar Foundation, to characterize the depth and geometry of the shallowest water table in large hyperarid hydrological basins in North Africa and the Arabian Peninsula. Herein, we describe the science objectives, measurement requirements, instrument design, expected performance, flight implementation scenarios, primary targets for investigation, and the first technology demonstration of the concept. Our performance analyses suggest that an airborne, nadir-looking sounding

Digital Object Identifier 10.1109/MGRS.2023.3338512
Date of current version: 1 March 2024

radar system operating at a 70-MHz center frequency with a linearly polarized folded-dipole antenna array—enabling a bandwidth (BW) of 50 MHz—and a surface signal-to-noise ratio (SNR) of 85 dB flying at an altitude of 500–2,000 m can map the uppermost water table depths of aquifer systems spanning tens of kilometers at a vertical resolution of 3 m in desiccated terrains to an average penetration depth of 50 m, with a spatial resolution of 200 m. For the first time, this airborne concept will allow time-coherent high-resolution mapping of the uppermost water tables of major aquifer systems in hyperarid areas, providing unique insights into their dynamics and responses to increasing climatic and anthropogenic stressors, which remain largely uncharacterized. The aforementioned significantly surpasses the existing capabilities for mapping shallow aquifers in these harsh and remote environments, which relies today on data collected on different timescales from sparse well logs that do not cover their geographic extents. A list of key abbreviations for this article can be found in "The Key Abbreviations Used in This Article."

INTRODUCTION

Understanding the impact of climate change on sea-level and groundwater resources directly affects the sustainability and socioeconomic stability of arid and hyperarid areas where groundwater is the primary source of irrigation and potable water. Consequently, the science associated with understanding the impacts of climate change on groundwater evolution is of paramount importance [1], yet, to this day, there are no developed experiments that allow large-scale mapping of aquifers in hyperarid areas such as North Africa and the Arabian Peninsula to understand their response to changing climatic and anthropogenic stressors.

Today, hyperarid environments, including cold/polar and warm deserts, represent ~10% of Earth's surface and continue to change in size under globally increasing aridity (e.g., [2]). Although polar ice sheets are continuously shrinking in size in response to global warming, hyperarid deserts are expanding by desertification [3].

In North Africa and the Arabian Peninsula, the drastic changes observed in water scarcity, quality, rainfall, flash floods, aquifer depletion, and accelerated desertification [4], [5] are all signs of substantial large-scale climatic variability in these areas resulting from global warming [6], [7], [8], [9], [10]. However, the aquifer systems in these areas are poorly characterized with regard to the impacts of climate change on their hydrological properties. The relationships between hydroclimatic variables—such as precipitation and evaporation rates from natural discharges, and transmission losses to aquifers—and the hydrological connections between surface water bodies and aquifers are poorly observed and modeled at the aquifer-system scale [11], [12], [13]. Furthermore, localized studies are often aimed at understanding small-scale or localized water resources, such that the

The Key Abbreviations Used in This Article

ADC: analog-to-digital converter
APIS: Aircraft power input system
ASTER: Advanced Spaceborne Thermal Emission and Reflection Radiometer
BW: bandwidth
CAD: computer-aided design
CCD: charge-coupled device
DAC: digital-to-analog converter
DC: direct current
DEM: digital elevation model
Desert-SEA: Desert Subsurface Exploration of Aquifers
DLR: German Aerospace Center
DNN: deep neural network
EM: electromagnetic
EMC: electromagnetic compatibility
EMI: electromagnetic interference
ESA: European Space Agency
FDEM: frequency-domain electromagnetic sounding
FM: frequency modulated
FPGA: field-programmable gate array
FZ: Fresnel zone
GPR: ground-penetrating radar
GPS: Global Positioning System
GRACE: Gravity Recovery and Climate Experiment
INS: inertial navigation subsystem
Lidar: light detection and ranging method
LNA: low-noise amplifier
MARSIS: Mars Advanced Radar for Subsurface and Ionospheric Sounding
PA: power amplifier
POC: proof of concept
PRF: pulse repetition frequency
PRI: pulse repetition interval
RAID: redundant array of independent disks
RF: radio frequency
RFES: RF Electronics Suite
RFI: radio-frequency interference
RMS: root-mean square
Rx: receiver/receive
SAR: synthetic aperture radar
SHARAD: Mars SHAllow RADar Sounder
SNR: signal-to-noise ratio
SRTM: Shuttle Radar Topography Mission
SSD: solid-state drive
STOL: short takeoff and landing
TRL: technology readiness level
Tx: transmitter/transmit
UHF: ultra high frequency
UWB: ultra-wideband
VHF: very high frequency
WGS: waveform generating subsystem

link to global or regional climate change is rarely addressed [8], [14] due to the absence of high-resolution, large-scale mapping techniques of the water tables in aquifer systems, which we address with this airborne mission concept.

The distribution and dynamics of groundwater in these areas are poorly known due to the paucity of subsurface measurements (i.e., well logs and geophysical prospecting) [12]. This lack of data limits the current understanding of the dynamic relationship between climate and groundwater and thus impedes the development of sustainable groundwater management in climate adaptation strategies [11]. Although ground-penetrating radars (GPRs) and drone-mounted radars are well suited for subsurface aquifer probing through desiccated desert sediments, they offer insufficient spatial coverage and limited penetration capabilities due to constraints on mass and power. Moreover, their deployment in the vast and harsh deserts of North Africa and the Arabian Peninsula is unfeasible from a logistical and operational point of view.

To address the aforementioned deficiencies, herein we propose an airborne desert subsurface exploration of aquifers (Desert-SEA) system using a high-power VHF sounding radar to map and characterize the top of the water table in shallow aquifer systems (i.e., <50 m deep). The proposed system will be able to perform mapping at the aquifer scale (i.e., a few tens to hundreds of kilometers), with meter-scale spatial and vertical resolutions in desert environments to improve the current understanding of Earth's paleoenvironment (i.e., previous wet periods that established aquifers that are today

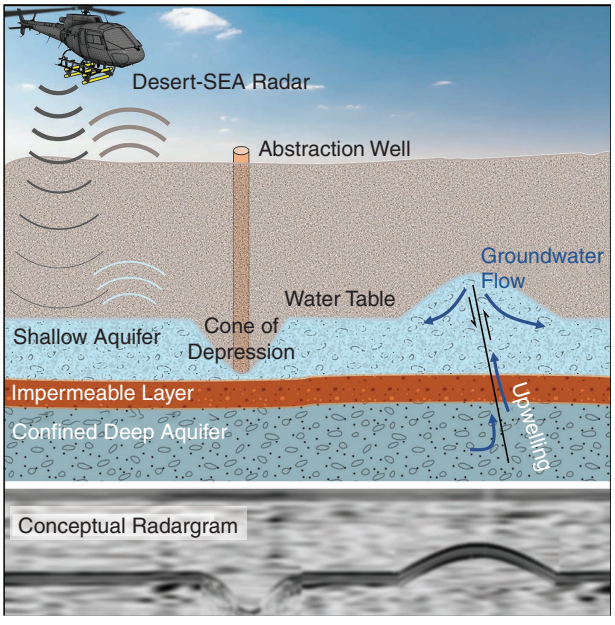

FIGURE 1. A conceptual graphic (not to scale) of the types of subsurface groundwater features detectable with Desert-SEA radar, along with their appearance on a radargram, including a flat water table, a cone of depression formed by extraction, and groundwater mounding caused by artesian upwelling from a deeper confined aquifer.

deep fossil ones) in terms of geographic variations in precipitation over extended epochs, groundwater inventories, and improved models of the evolution of Earth's water cycle.

The measurements by Desert-SEA (see Figure 1) will characterize key desert areas to inform on the discharge and recharge processes in fossil aquifer systems and establish critical constraints for understanding both present and past hydrological cycles and the impacts of paleoclimatic changes (i.e., precipitation) on these systems. In particular, Desert-SEA will provide crucial insight into the groundwater resources in hyperarid deserts, which account for the largest fossil aquifer systems worldwide and where techniques used to explore groundwater on a large scale remain underdeveloped [15]. Furthermore, the application of Desert-SEA's data to water resource management aligns well with the leading socioeconomic priorities of arid and hyperarid areas [5], [16], [17], [18].

MAPPING SHALLOW AQUIFERS

Today, deserts in North Africa and the Arabian Peninsula are some of the harshest and most arid climates on Earth [2], with almost half of their surfaces receiving less than 100 mm of annual precipitation [19], [20]. However, during the last 1 million years, these deserts have experienced multiple periods of enhanced precipitation and aquifer recharge, leading to the occurrence of deep aquifers that are no longer recharged (i.e., fossil aquifers), with substantial water storage [21]. These deep aquifers (formed during wetter paleoclimatic conditions) recharge shallow aquifers through artesian upwelling along geological discontinuities [22], leading to the formation of groundwater mounds near the desert surface [12]. Examples of these major transboundary aquifers include the Nubian Sandstone Aquifer System (2.6 million km^2) between Egypt, Libya, Sudan, and Chad; Northwestern Saharan Aquifer system (2.1 million km^2) between Libya, Algeria, and Tunisia; and Upper Mega-Aquifer System (1.6 million km^2) between Saudi Arabia, Qatar, the United Arab Emirates, Jordan, Bahrain, and Kuwait (see Figure 2) [12], [16]. These aquifers have a striking similarity in their lithological composition (i.e., deep sandstone aquifers underlying shallow carbonate ones, with thick shale aquitards between them), climatic conditions (i.e., very limited precipitation), high structural control, and abundant features of surface/near-surface discharge of deep fossil groundwater [22], [24], [25].

Desert-SEA will explore climate change signatures in the subsurface of hyperarid regions by leveraging its unique airborne radar-sounding capabilities to address long-standing science questions about groundwater dynamics in remote deserts.

UNCERTAINTIES WITH AQUIFERS' SPATIAL CHARACTERISTICS

Desert-SEA's overall science goal is to construct detailed maps of the spatial distribution of shallow aquifers in Earth's hyperarid areas to better understand desert

hydrology and enhance flow models to provide new insights into recent and past changes in these aquifers and their implications for groundwater sustainability. The urgent need to quantify the distribution and dynamics of fossil aquifers in hyperarid areas is summarized by the following open science questions.

HOW DO DEEP AND SHALLOW AQUIFERS CONNECT IN HYPERARID AREAS?

Given the hyperarid conditions that prevail in core deserts (i.e., the inland part, not along coastlines) like the Saharan–Arabian Desert, modern recharge to its aquifers is limited to coastal areas, where a relatively consistent pattern of precipitation replenishes fossil water storage in these mega aquifers [7], [26]. In desert core regions (i.e., the overwhelming majority of the area occupied by the Saharan–Arabian Desert), the sole source of recharge to the shallow aquifers is the artesian upward leakage from deep aquifers along vertical/subvertical faults [22], [27]. The specific characteristics of the faults along which deep water is channeled vertically are still to be identified due to the lack of hydrological datasets and the difficulty of conducting large-scale geophysical measurements under such remote, harsh, and hyperarid conditions. Recently, the groundwater mounding phenomenon was proposed as a diagnostic feature to delineate the locations of aquifer connectivity between deep and shallow ones [12]. Detecting these features helps define the characteristics of the fault systems that control the recharge to shallow aquifers from deeper ones in the desert core. Integrating isotopic, hydrological, and geoelectrical datasets has proven to be a valuable tool for delineating groundwater mounds in hyperarid deserts [12], yet, the limited spatial capabilities of geophysical measurements and limited well distribution impede large-scale mapping of these features.

Desert-SEA and similar VHF sounding radar missions can probe shallow aquifers (<50 m deep) under arid conditions, e.g., using a 45-MHz center-frequency radar sounder with a 10-MHz BW [15], and thus, they provide the unique opportunity to perform large-scale and time-coherent geophysical measurements to delineate the groundwater mound geometry as well as assess their origin and dynamics and ultimately provide large-scale mapping of the shallow fossil aquifers in the desert core that cannot be achieved using sporadically distributed well logs that are concentrated near urban areas. The change in depth of the water table or the vadose zone due to high moisture over areas spanning a few kilometers should be able to generate sufficient dielectric contrast in the first few tens of meters [28], [29] to be measured from both airborne or orbital sounding radars using radiometric analysis of the surface reflected signals or analysis of returned echoes from subsurface interfaces.

WHAT ARE THE DEPTHS AND SPATIAL ATTRIBUTES OF SHALLOW FRESHWATER AQUIFERS IN HYPERARID AREAS?

In many hyperarid areas worldwide, sporadic precipitation occurs over mountainous areas and is channeled through expansive watersheds as surface runoff and groundwater flow. Because some watersheds collect precipitation over large areas that are channeled through a few main valleys, substantial amounts of freshwater can either form or recharge aquifers beneath these valleys, with flow preferentially channeled (or obstructed) by faults, shear zones, and dikes. Given natural variations in local geology and meteorology, large variations are expected in the amount of local surface runoff, infiltration, and groundwater recharge from one valley to another [30]. These factors cause substantial uncertainties in the occurrence and extent of modern shallow aquifers throughout hyperarid areas. The penetration capabilities of Desert-SEA can help map the distribution of shallow aquifers in the Saharan–Arabian Desert, where the water table is typically less than 50 m deep in most of these alluvial aquifers [26], [31], [32].

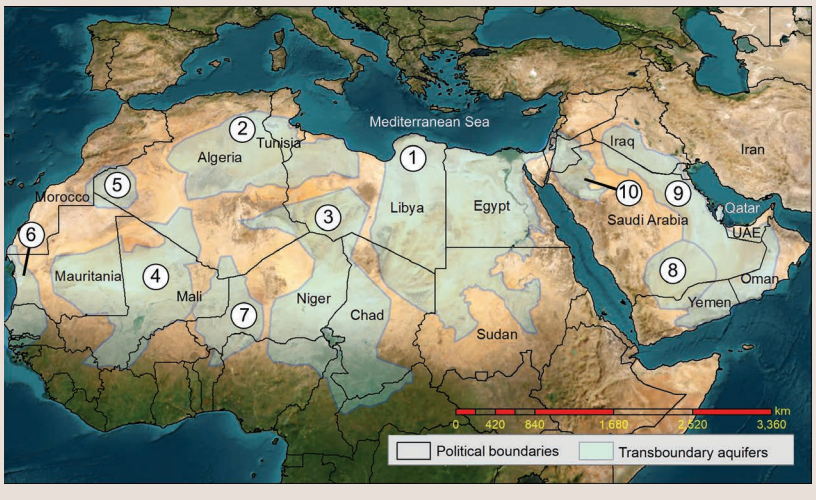

FIGURE 2. The notional distribution of transboundary fossil aquifers in North Africa and the Arabian Peninsula. Notional locations are based on data from Abotalib et al. [22] and the International Groundwater Resources Assessment Centre [23]. Boundaries of the aquifers and the occurrence of shallow water are poorly constrained due to the limited number of well logs available. Desert-SEA addresses this problem by providing an unprecedented dense subsurface mapping of shallow aquifers, especially near recharge and discharge areas. Small domestic aquifers not crossing country boundaries are not shown. The aquifers include ① the Nubian Sandstone aquifer, ② North Western Saharan aquifer, ③ Lake Chad basin aquifer, ④ Taoudeni basin aquifer, ⑤ Tindouf aquifer, ⑥ Senegalo–Mauretanian basin aquifer, ⑦ Irhazer–Illuemeden basin, ⑧ Wajid aquifer, ⑨ Saq-Ram Aquifer System, and ⑩ Umm er Radhuma–Dammam aquifer.

WHERE ARE THE STREAMS OF MAJOR PALEO RIVERS IN THE SAHARAN–ARABIAN DESERT?

During previous geological times, the Saharan–Arabian Desert witnessed numerous pluvial episodes when annual precipitation exceeded 1,500 mm during the Oligocene and Miocene time, forming widespread forests that are indicated by the vast distribution of petrified woods and extensive river sediments [33], [34]. Even during the Quaternary Period (i.e., tens to hundreds of thousands of years ago), the Saharan–Arabian Desert witnessed alternation between wet and dry climatic episodes [7], and, during the wet episodes, a vast river network flowed over the then-steppe or savanna-covered terrains [35]. Numerous efforts have been exerted to map the distribution of these paleo rivers using satellite radar imaging, which have been referred to as *radar rivers*, such as in North Africa [36], [37], Western Sahara [38], and the Arabian Peninsula [39]. However, most of the areas once covered by rivers are currently obscured by thick, wind-blown sand dunes and sand sheets with thicknesses exceeding the maximum (max) penetration capabilities of current orbital radar missions. These paleo rivers represent ideal conditions for the occurrence of shallow aquifers as they can retain meteoritic freshwater atop a bed of highly impermeable material much closer to the surface. They are typically distinguished by two hydrogeological units: channel fills and floodplains, where channel-fill sediments typically contain fewer clays and usually transport lower-salinity water compared to the floodplain sediments [40]. The facies change among channel-fill deposits (i.e., dominated by sand and gravels), and floodplain sediments (dominated by a mixture of sands and clays) can be used to distinguish between the two units using geoelectrical measurements [41] as well as radar-sounding techniques [29], [42]. Mapping the distribution of these paleo rivers with an emphasis on the channel-fill sediments has substantial value for understanding the aquifer distribution in these systems, even for those residing beneath the penetration limit of radar-sounding techniques.

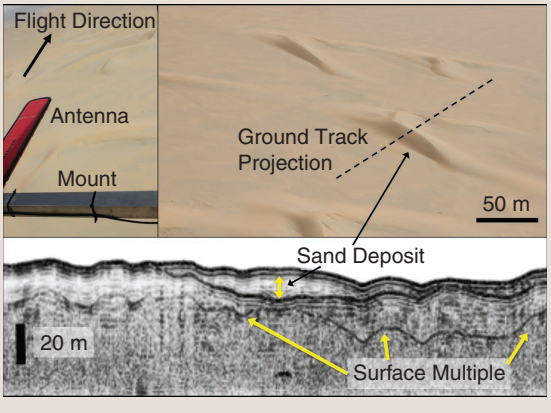

FIGURE 3. Airborne 40-MHz VHF radar subsurface mapping of the thickness of the dunes (~15 m) in the Kuwait desert. Desert-SEA provides similar data from an airborne platform for large regions that exceed the coverage capabilities of ground surveys. This full profile is about 200 m in length.

DESERT-SEA OBJECTIVES

Desert-SEA is a scientific investigation and a technology development project with four well-defined objectives that address the aforementioned science questions, and will thereby directly improve our understanding of aquifer dynamics and signatures of climate change in hyperarid regions—one of Earth's least understood environments due to the lack of large-scale mapping investigations:

MEASURE THE DEPTH OF THE WATER TABLE IN SHALLOW AQUIFERS AND ITS SPATIAL VARIABILITY

The current delineation of aquifer systems and water table depths is based on sporadic well logs from widely spaced wells (see Figure 2). We will use the reflected amplitude and time delay associated with subsurface radar reflections to determine the local depth of the water table. At the top of the water table (the capillary zone), the dielectric contrast among sediments in dry and saturated conditions is capable of producing strong returns (e.g., [29] and [43]). Therefore, GPRs have been widely used for shallow (<50 m deep) and local hydrogeophysical studies [44]. 2D radargrams (2D cross sections of subsurface energy reflections) allow measurement of the depth to the water table (e.g., [45]), distribution of faults that control groundwater flow [7], and delineation of the recharge and discharge areas [46], [47]. Figure 3 shows 40-MHz airborne radar-sounding data (not corrected to topography) in the northern desert of Kuwait performed by NASA's Jet Propulsion Laboratory during May 2011 [48]. Here, the base of the dunes at ~15 m in depth, overlaying partially saturated sand, appears as strong subsurface reflectors along the flight track of the investigated area. An example of these sand deposits is visible in the central part of the radargram. Multiples of the surface reflection (i.e., clutter due to multiple bounces between the bottom of the helicopter and the ground) are also present, but easily distinguished from true subsurface reflectors in this case due to the flat surveyed topography, since their pattern is identical to the surface one. Desert-SEA, with its dense coverage over targeted areas in the Sahara and Arabian Peninsula, will extend the scale of these experiments to construct regional maps showing the spatial variations of water levels over large aquifer systems as well as along the main ephemeral valleys (normally dry but episodically active riverbeds). It will also allow the delineation of potential buried large paleochannels that represent paleo-recharge areas [37], [49], [50], [51], [52]. Such large coverage, required to explore the hydrogeology of this extensive area, is unachievable using GPRs and other traditional methods [i.e., drilling or vertical electrical survey, or transient electromagnetic (EM) methods].

IDENTIFY HYDRAULIC GRADIENTS AND GEOLOGIC STRUCTURES CONDUCIVE TO OR HINDERING GROUNDWATER RECHARGE, FLOW, AND DISCHARGE

In areas that experience frequent precipitation, the water table's shape and the groundwater flow pattern are strongly influenced by the local topography, making any evidence of regional or interbasin flow challenging to recognize. However, in arid regions, the long intervals between rain events often provide sufficient time for correlation of the shape of the water table with topography to decay, making evidence of large-scale hydraulic continuity considerably easier to identify [53]. For this reason, the best-recognized examples of regional groundwater flow on Earth are all found in arid environments.

The flow of underground water generated by the hydraulic gradient is the most fundamental element used to characterize a groundwater system. Desert-SEA's 2D radargrams, with a minimum of 100-m ground-track spacing, will provide unprecedented spatial coverage (closer spacing would be redundant considering that these features span multiple kilometers) for mapping the distribution of water levels in shallow aquifers at 3-m-scale vertical resolution (to observe the gradual variations in water table depth associated with mounding). This will result in the first comprehensive picture of spatial variations in the hydraulic head for the world's largest, but least understood, hyperarid aquifer systems.

Using hydraulic gradient data measured by Desert-SEA, integrated with local currently available in situ geophysical data, we can map 1) regional and local recharge and discharge spatial domains, 2) spatial variation of water table depth on the regional scale, and 3) the geologic features associated with abrupt gradient changes serving as hydraulic conduits or barriers. This knowledge gained from Desert-SEA's data considerably surpasses traditional in situ geophysical methods.

COMBINE RADAR-SOUNDING OBSERVATIONS WITH THE AVAILABLE IN SITU GEOPHYSICAL DATASETS OF FOSSIL AQUIFERS TO PROVIDE INSIGHTS INTO THEIR HYDROGEOLOGIC EVOLUTION

Desert-SEA's observations will be integrated with geologic, hydrologic, topographic, geochemical, and isotopic datasets to understand past (paleo) recharge regimes through the examination of water table depth and flow regimes (e.g., [12]). Specifically, with Desert-SEA's measurements, we will be able to identify areas that have received local precipitation or were fed by paleochannel networks during previous more humid climate conditions. These are known as *paleo-recharge domains*. Coupled with our new knowledge of the areas contributing to present-day recharge, groundwater flow models can be significantly enhanced, enabling more accurate simulations of the hydrologic evolution of the regional aquifer system from more humid paleoclimatic conditions to the present day [54].

These results will help us 1) estimate spatial and temporal paleoclimatic changes, 2) evaluate how modern surface-water features and human activities affect the fossil groundwater system, and 3) more accurately project the potential impact of future climatic changes on the depletion of these aquifers due to excessive man-induced exploitation and natural discharge [16], [55]. In addition, Desert-SEA examination of the hydrogeology of present-day Saharan and Arabian hyperarid environments can have direct relevance to our understanding of groundwater dynamics in regions that may change from semiarid to arid or hyperarid regimes in response to climate change, such as the Southwestern United States [56], [57].

DETERMINE SHALLOW GROUNDWATER SALINITY BY COMBINING SOUNDING RADAR AND FREQUENCY-DOMAIN EM INDUCTION SOUNDING DATA

Desert-SEA's sounding radar data will also be used to estimate propagation losses to the top of the water table to identify anomalous subsurface radar absorption, which can be attributed to the presence of brackish water-saturated zones. Additional observations by a towed-bird frequency-domain EM (FDEM) induction sounder can yield vertical resistivity data and hence assess groundwater salinity with a vertical resolution of a few meters to tens of meters to a depth of 100 m to support the interpretation of radar observations (e.g., [58], [59], and [60]).

The expected outcome of the Desert-SEA project is to provide the first large-scale, high-resolution, hydrogeological maps of specific areas witnessing heightened groundwater dynamics (i.e., recharge or discharge) in the North African Sahara and the Arabian Peninsula, hence exploring one of the least characterized water budgets of our planet.

SCIENCE MEASUREMENT AND INSTRUMENT REQUIREMENTS

Desert-SEA's science goals can be achieved using a single airborne VHF sounding radar to penetrate dry desert sediments and explore the spatial and structural characteristics of shallow aquifers in the first 50 m [12], [42].

Four main interrelated factors drive the instrument requirements for Desert-SEA: 1) maximize the penetration depth, 2) probe the subsurface with a vertical resolution of ~3 m, 3) reduce the radar's vertical blind zone, and 4) reduce the size of the radar's footprint to mitigate surface clutter. Combined, these factors enable an accurate assessment of the depth of the water table, aquifer delineation, the overlying sediment lithology, and the identification of groundwater conduits.

To achieve the science goal (G1) and objectives (S1–S4) detailed in the "Desert-SEA Objectives" section and laid out in the first two columns of the science traceability matrix in Table 1, Desert-SEA needs to measure the surface and subsurface dielectric contrasts (PP1) and the associated two-way subsurface attenuation (PP2) in the radar signal to assess water saturation associated with the top of the water table and structural discontinuities as potential groundwater conduits. The latter are determined

TABLE 1. THE SCIENCE TRACEABILITY MATRIX.

DESERT-SEA SCIENCE GOALS (SOUNDING RADAR ONLY) (G)	SCIENCE OBJECTIVES (S)	SCIENCE MEASUREMENT REQUIREMENTS PHYSICAL PARAMETERS (PP)	SCIENCE MEASUREMENT REQUIREMENTS OBSERVABLES (Obs)	INSTRUMENT REQUIREMENTS MINIMUM (IR)	INSTRUMENT REQUIREMENTS PROJECTED (PIR)	MISSION REQUIREMENTS (TOP LEVEL) (MR)
G1: construct detailed maps of the spatial distribution of shallow aquifers in Earth's hyperarid areas to better understand desert hydrology and enhance flow models in support of sustainable transboundary resource management in North Africa and the Arabian Peninsula under anthropogenic and climatic stressors.	**S1:** measure the depth of the water table in shallow aquifers and its spatial variability. **S2:** identify hydraulic gradients and geologic structures conducive to or hindering groundwater recharge, flow, and discharge. **S3:** combine radar-sounding observations with the available in situ geophysical datasets of fossil aquifers to provide insights into their hydrogeologic evolution. Range: 0–50 m (20 m) deep. Spatial resolution: 100-m along track and 300-m across track (radar surface footprint). Vertical resolution: ± 3 m. Detection accuracy: saturation of 10% water by volume.	**PP1:** determine spatial and vertical changes in the dielectric properties of the probed ground for contrasts >10%. **PP2:** determine the subsurface attenuation in decibels/meters (due to dielectric losses and volume scattering).	**Obs1:** return signal timing of continuous surface and subsurface reflectors (inferred to be the stratigraphy and water table interface echoes) in the first 50 m (20 m) at 3-m vertical resolution, sampled at 100-m along track and 300-m across track (<3-dB precision) [PP1]. **Obs2:** return signal strength of the surface, stratigraphy, and water table interface echoes (0–50 m, 100 × 300 m, <3-dB precision) [PP2].	**IR1:** 50-MHz (50-MHz) radar BW [Obs1]. **IR2:** 80-dB (50-dB) surface SNR or better [Obs1 and Obs2]. **IR3:** 3-dB (3-dB) radiometric accuracy [Obs1 and Obs2]. **MINIMUM PERFORMANCE (Pf)** **Pf1:** 50-m (20-m) penetration depth. **Pf2:** <15-m (<15-m) vertical subsurface blind zone. **Pf3:** 3-m (3-m) vertical resolution. **Pf4:** 300 × 300-m (300 × 300-m) spatial resolution (radar surface footprint).	**PIR1:** 50-MHz (50-MHz) radar BW [Obs1]. **PIR2:** 80-dB (80 dB ± 3 dB) surface SNR or better [Obs1 and Obs2]. **PIR3:** 3-dB (3-dB) radiometric accuracy [Obs1 and Obs2]. **PROJECTED PERFORMANCE (PPf)** **PPf1:** 70-m (25-m) penetration depth [62]. **PPf2:** <10-m (<10-m) vertical subsurface blind zone. **PPf3:** 3-m (3-m) vertical resolution. **PPf4:** 20-m along-track × 400-m across-track (20-m × 400-m) spatial resolution (radar surface footprint).	**MR1:** flight altitude of 500–2,000 m [Pf2]. **MR2:** 50% duty cycle for data acquisition to ensure dense coverage with high SNR of surveyed areas [PIR2]. **MR3:** ground-track spacing ≤5 km over 90% of targeted basins. **MR4:** geolocation (knowledge) of along-track nadir footprint of radar to ± 10 m to support declutter. **MR5:** operating in areas with topographic root-mean-square height variation (h_{rms}) below 2 m within the radar surface footprint (see the "Desert-SEA Objectives" section.)

*Nominal values correspond to the full flight model operating at a 70-MHz center frequency; parenthetical values "()" correspond to the proof-of-concept model that operates at a 200-MHz center frequency.

from the return signal timing (Obs1) and return signal strength (Obs2) in the 2D radargrams generated by Desert-SEA (e.g., in Figure 1).

To achieve the above, the Desert-SEA's radar system needs to employ a frequency BW of 50 MHz centered at 70 MHz (IR1) with a 3-dB directive antenna, an effective SNR at the surface of at least 80 dB (post-processing) (IR2) [42], and a radiometric accuracy of 3 dB (IR3). Together, these yield an optimal tradeoff of penetration depth (Pf1), vertical blind zone (Pf2), vertical resolution (Pf3), and radar footprint size with a minimum spatial resolution of 300 × 300 m (Pf4) [12].

The full characteristics of a radar system that can meet these science measurement requirements are summarized in the right-most columns of Table 1 and fully detailed in Table 2. It is important to note that Desert-SEA will only operate over smooth, flat basins—where shallow aquifers are formed—with root-mean-square height variation (h_{rms}) of less than 2 m within the radar's footprint to maximize the signal-to-clutter ratio (MR5) [42].

INITIAL SCIENCE MISSION

The initial deployment of the Desert-SEA airborne project will consist of only the radar sounder, while enhanced mission options include off-the-shelf optical charge-coupled device (CCD) and thermal cameras, lidar, and a towed-bird FDEM.

The initial Desert-SEA deployment will provide the first time-coherent maps of specific areas witnessing heightened aquifer dynamics, i.e., recharge or discharge sites, due to anthropogenic and climatic drivers. Its 200-m horizontal resolution will provide a substantial improvement in delineating aquifers over the orbital gravimeter Gravity Recovery and Climate Experiment's (GRACE's) horizontal resolution of a few hundred kilometers [61], and over water table depth measurements from sporadic well logs (see Figure 2). In addition, Desert-SEA's initial deployment will provide the first dataset that addresses the hydrogeological cycle of such expansive deserts. The "Targeted Study Sites" section details the initial targets of interest for this investigation.

DESERT-SEA INSTRUMENT

RADAR SYSTEM DESIGN

The Desert-SEA's radar system is a VHF low-band radar sounder intended to initially operate on a rotary wing aircraft between 500 and 2,000 m above ground level. A functional block diagram of the radar system is presented in Figure 4. The principal characteristics that guide the radar design and its implementation are presented in Table 2, and

the measurement geometry is depicted in Figure 5. Here, we briefly overview the underlying parameters of each design requirement.

- *Center frequency*: We chose a center frequency of 70 MHz with a chirp BW of 50 MHz (45–95 MHz). These parameters offer a balanced tradeoff between meeting science requirements and implementation and flight constraints, i.e., between antenna size and nominal penetration depths. A lower frequency provides less subsurface attenuation and deeper penetration, but an antenna with a required 3-dB directivity to minimize surface clutter may be too large for the aircraft. On the other hand, a higher frequency would permit a reasonable antenna size, but the higher subsurface attenuation limits penetration depth. It is important to note that the system is deployed in remote, nonurban areas away from frequency-modulated transmissions, and therefore will not interfere with the 88–95-MHz frequency band utilized by public radio services.
- *Vertical and spatial resolutions*: To meet the vertical resolution requirement of 3 m in dry sand, we designed the radar electronics subsystems to have a 50-MHz chirp BW. Along-track and cross-track resolution of the subsurface return is commensurate with the scale over which the nadir signal is coherent, i.e., the Fresnel zone (FZ) radius of $\sqrt{\lambda h/2}$, where λ is the wavelength and h is the altitude. For example, for an altitude of 1,000 m and a frequency of 45 MHz (λ = 6.66 m) and 95 MHz (λ = 3.15 m), the FZ radii, corresponding to the half-power spatial resolutions for a surface that is smooth with respect to the wavelength, are approximately 58 and 40 m, respectively. Synthetic aperture radar (SAR) processing provides finer along-track resolution of the surface returns (of the order of 10-15 m) for rejecting off-nadir surface clutter. Cross-track resolution of the surface returns, assuming a surface that is rough with respect to the wavelength, is approximately twice the range-resolution-limited patch radius, which is $\sqrt{2h\rho_r}$, where ρ_r is the range resolution in air.
- *Antenna polarization*: Desert-SEA will use horizontal linearly polarized folded-dipole array antennas mounted along the track (i.e., colinear with the helicopter's fuselage) to minimize its impact on the aircraft's aerodynamics.

To meet the aforementioned design requirements, Desert-SEA's radar is composed of the following seven subsystems.

POWER DISTRIBUTION SUBSYSTEM

The power distribution system has an aircraft power input system (APIS). The APIS system filters and protects the aircraft's 24-V dc power supply from Desert-SEA's power faults. It also isolates the Desert-SEA radar from aircraft EMI and over-voltage conditions. The internal radar power system consists of primary and redundant systems intended to nominally operate in high temperature environments for extended periods. The radar is expected to

TABLE 2. SUMMARY OF DESERT-SEA RADAR CHARACTERISTICS.

PARAMETER	VALUE	UNITS
Scenario:	—	—
Radar height above terrain	500–2,000	m
Diameter of nearest illuminated patch at 1,000-m altitude, range-resolution limited (for noncoherent scatter)	200	m
Diameter of nearest illuminated patch at 1,000-m altitude, Fresnel reflection zone limited (for coherent reflection)	47	m
Radar tangential velocity (helicopter)	80	kn
Radar waveform:	—	—
Operating frequency range, nominal	45–95	MHz
Waveform BW	≤50	MHz
Waveform center frequency (BW dependent)	50–70	MHz
Pulsewidth (variable; altitude dependent)	1–5	μs
Intrapulse modulation	linear FM	—
Pulse repetition frequency	10–20	kHz
Antenna:	—	—
Gain per antenna (dipole + reflector) (nominal)	−2–0	dBi
Beamwidth, along track, half-power, one way (nominal)	~90	—
Beamwidth, across track, half-power, one way (nominal)	~90	—
Tx:	—	—
Power amplifier RF output power (peak)	200–500	W
Tx RF duty factor (waveform dependent)	≤10	%
Total Tx RF loss (T/R switches, cables, and so on)	4.5	dB
Rx:	—	—
Total Rx RF loss (T/R switches, cables, and so on)	5.5	dB
LNA noise figure (for a high dynamic range LNA)	1.5	dB
Rx system noise figure	7	dB
Rx system effective noise temperature (excluding external noise)	1,163	K
Range processing:		
Range resolution in air without weighting (for a 50-MHz BW)	3	m
Range resolution in air including Tx and Rx weighting for range sidelobe control	5	m
Depth resolution in subsurface medium with $\varepsilon_r = 3$ (velocity factor = 0.58)	2.9	m
Along-track processing:		
Along-track SAR resolution	13–26	m
Synthetic aperture integration angle	5.3–10.6	degrees
Synthetic aperture length (at height = 1,000 m)	93–185	m
Synthetic aperture time (at 80 kn; height = 1,000 m)	2.25–4.5	s
Presum ratio (coherent integration per along-track sample, typical)	200	pulses

FM: frequency modulated; LNA: low-noise amplifier.

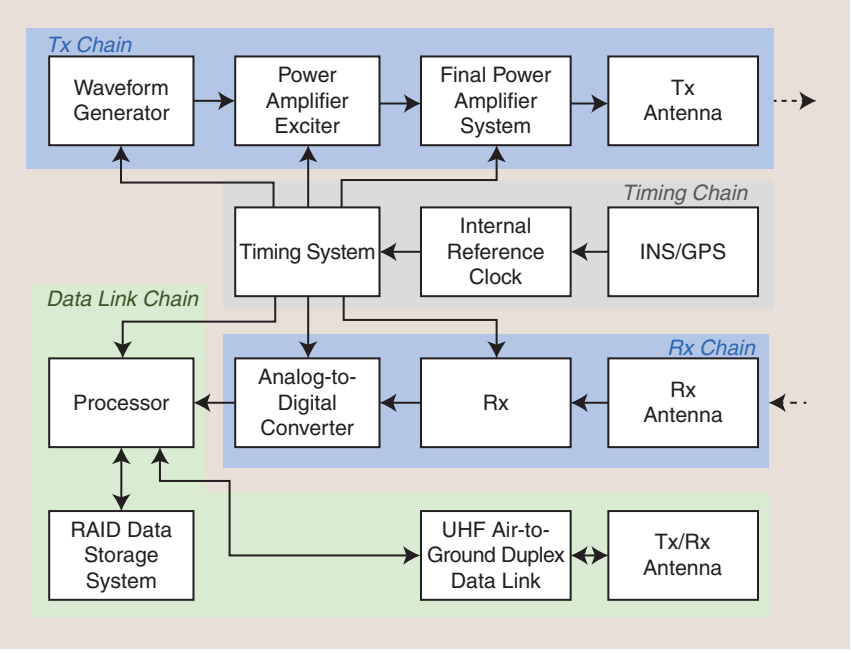

FIGURE 4. The Desert-SEA radar functional block diagram. INS/GPS: inertial navigation system/GPS; UHF: ultrahigh frequency; RAID: redundant array of independent disks.

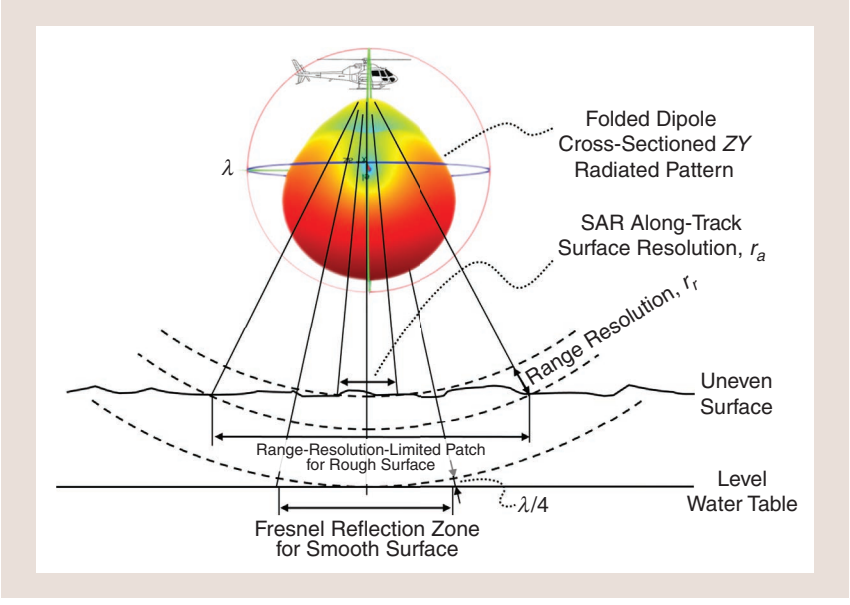

FIGURE 5. The Desert-SEA radar measurement geometry. SAR: synthetic aperture radar.

require about 1 kW of prime power from the aircraft.

TRANSMITTER CHAIN

The transmitter (Tx) chain consists of six core components (see Figure 6). In general, a field-programmable gate array (FPGA) and digital-to-analog converter (DAC) generate the shaped Tx waveform signal, which is amplified by the power amplifier (PA) and filtered to reduce spectrum interference. The flight PA will be a suite of lower PAs that provide increased reliability and efficiency. The following is a brief description of each component:

- *Waveform generating subsystem (WGS)*: The WGS is an FPGA-based arbitrary waveform generator that provides multiple shaped waveforms used for radar emission and internal calibration. Figure 7 provides an example of the type of weighted waveform before and after pulse compression, which is used for subsurface penetration and range sidelobe suppression.
- *PA driver*: The low-level WGS signal at 1 mW (0 dBm) is amplified to a 40-dBm level anddivided into four equal 2-W (33-dBm) signals, which then drive the Desert-SEA's 500-W peak PA assembly.
- *500-W peak PA*: For redundancy and reliability, the sounder's PA uses four independent 125-W peak amplifiers. Each amplifier is individually controlled and monitored. In the event of an amplifier failure, the remaining amplifier complement will allow mission completion.

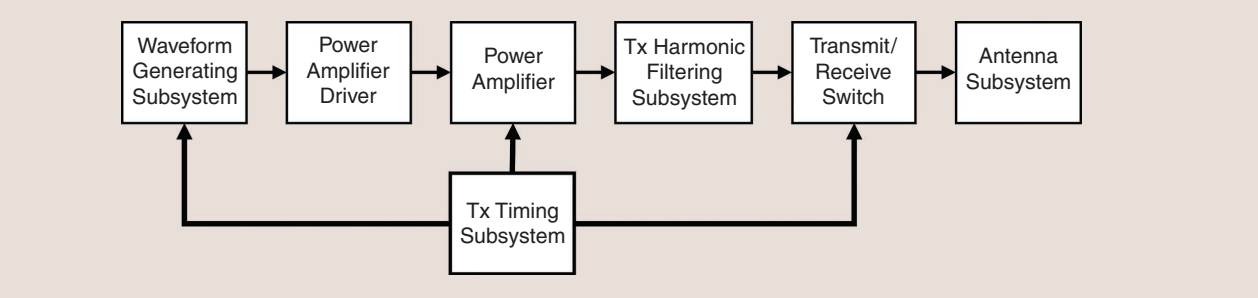

FIGURE 6. The Tx chain block diagram.

- *Tx timing subsystem*: Parallel operation of individual PAs requires a precision timing subsystem to synchronously control each amplifier. This will be done with a high-speed FPGA from Xilinx. A rubidium clock disciplined to a one-pulse-per-second GPS clock is used to produce the fundamental radar clock.
- *Tx harmonic filtering subsystem*: The harmonic filter substantially attenuates Tx harmonics above 100 MHz. It is required to minimize EM interference (EMI) in the VHF and ultrahigh-frequency (UHF) aviation bands and provides EM compatibility with the host aircraft.
- *Transmit/receive (T/R) switch*: The Desert-SEA's radar operates at a relatively high power (500 W), high pulse repetition frequency (PRF), and 5-μs Tx pulse duration. Custom T/R switch solutions will be designed, built, and tested to provide 500-ns switching times and controlled insertion loss of <1.25 dB.

RECEIVER CHAIN

The Desert-SEA Receiver Chain consists of the following two major subsystems, as depicted in Figure 8:

- *Rx limiter and timing subsystem*: The limiter attenuates Tx signal leakage into the sensitive Desert-SEA's receiver (Rx) and controls the overall Rx chain while listening for signal returns.
- *Multistage Rx gain stages*: Three cascaded, switchable gain stages provide 20–60-dB gain over the 45–95-MHz fixed-gain band. The high and low gain stages precede the analog-to-digital converter (ADC) and embedded FPGA processor.

TIMING SUBSYSTEM

The Desert-SEA Timing System (see Figure 9) orchestrates in precise detail the collective performance of Desert-SEA's internal subsystems, as first introduced in the "Transmitter Chain" section.

Powered by an industry-standard Xilinx FPGA and synchronized by high-precision GPS signals, the FPGA provides the fundamental system cadence to initialize the string of events required to generate the specialized Tx waveform, amplify it to a level sufficient to deeply penetrate Earth's surface, and start a process to accurately measure the time delay to the surface and subsurface reflectors.

INERTIAL NAVIGATION SUBSYSTEM/GPS SUBSYSTEM

Desert-SEA's inertial navigation system (INS)/GPS system, mounted on the antenna support structure, provides location, velocity, and timing information, which are time-stamped alongside the radar's return and telemetry data. This information is used for motion compensation in the SAR's processing and is also applied to the processed radargrams to provide depth and along-track metrics.

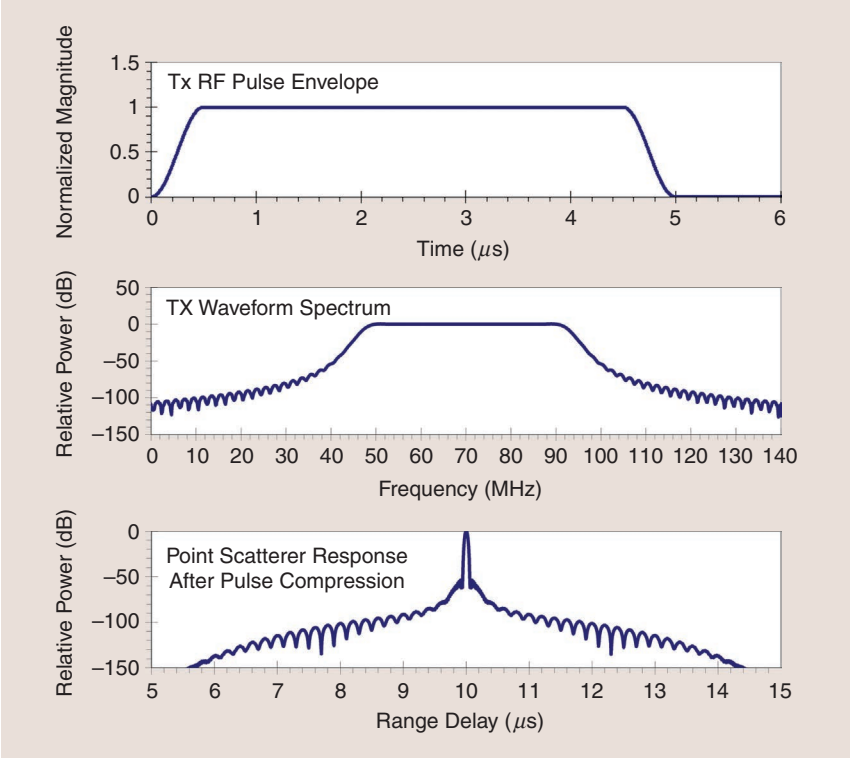

FIGURE 7. Desert-SEA waveform characteristics in the time and frequency domains.

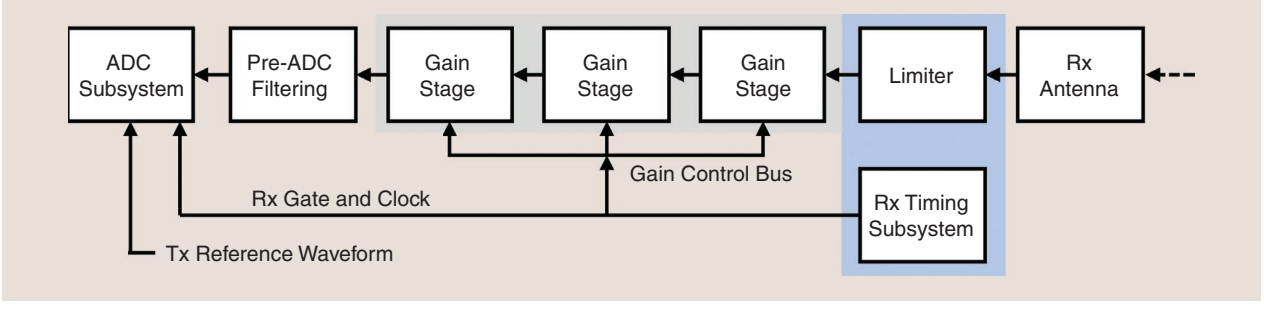

FIGURE 8. The Rx chain block diagram (one of two channels shown).

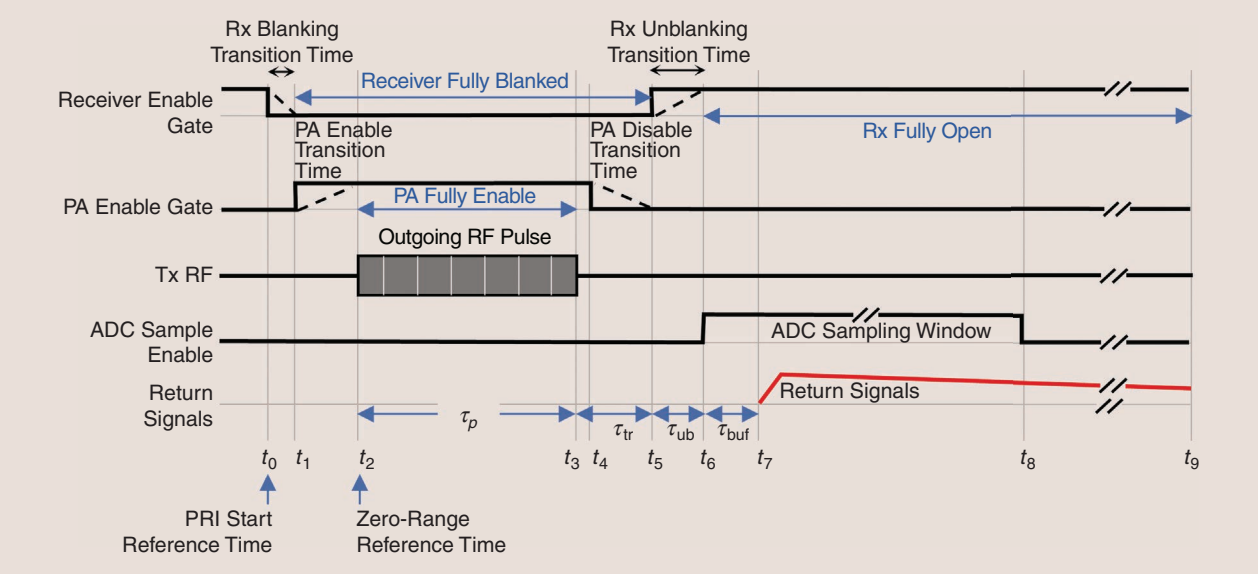

FIGURE 9. T/R signal timing. PRI: pulse repetition interval.

The INS/GPS provides measurements of position, velocity, and altitude at an update rate of 400 Hz. The INS/GPS also provides a primary timing signal, which disciplines Desert-SEA's master clock to an accuracy of 30 ns (root-mean square).

SYSTEM PROCESSOR AND DATA CHAIN

Desert-SEA utilizes a multicore embedded processing system that operates with a Linux operating system. Secondary processing units communicate over internal USB 3.0 fiber and Ethernet interfaces to transport control, monitoring calibration and ground data link information. The components of the system processor and data chain are listed as follows:

- *Multichannel ADC*: The ADC transforms the wide-dynamic antenna range return signals into 14-bit digital words that are filtered and stored for postflight processing.
- *Redundant array of independent (RAID) solid-state drive (SSD) subsystem*: Radar return data [level 0 (L0)], along with telemetry data, will be encoded on a minimum of two physical terabyte RAID SSDs. The radar data rate to the SSD subsystem is calculated in Table 3.
- *Telemetry subsystem*: A telemetry monitoring and reaction system consisting of multiple power, current, voltage, temperature, and strain gauge sensors will be located within the RF Electronics Suite (RFES) and antenna support platform to continuously sample and evaluate the status of critical Desert-SEA subsystems (e.g., Tx power output, voltages, temperatures, and so on) to maintain nominal operation and aircraft and personnel safety. Telemetry data will be continuously logged on the RAID subsystem for postmission analysis.
- *Broadband air-to-ground link*: A two-way UHF broadband radio provides Desert-SEA ground operators with a full-duplex 40–60-Mbit/s link to monitor unprocessed radar data for quality control, and reconfigure radar parameters that are scenario dependent (e.g., altitude- and speed-dependent ones).
- *Calibration subsystem*: Desert-SEA's system processor and data chain employs the following three calibration modes:
  1) *Premission all system calibration*: This mode automatically injects test signal vectors into key subsystem components, such as the Rx, and subsequently measures, compares, and adjusts the system under test to meet a predetermined metric.

TABLE 3. THE DESERT-SEA RADAR OUTPUT DATA RATE CALCULATION.

PARAMETER	VALUE	UNITS
ADC sample rate	300	Msps
Bits per ADC sample (max)	16	bits/ADC sample
PRF (max)	20,000	Hz
PRI (min)	50	μs
ADC sampling window for sounding	8	μs
ADC sampling window for RFI sensing	8	μs
ADC sampling window for calibration	4	μs
Total sampling time per PRI	20	μs
Total ADC samples per PRI	6,000	ADC samples/PRI
Presum ratio	100	pulses/along-track sample
Effective along-track sample rate	200	along-track samples/s
Presummed samples per second per Rx channel	1,200,000	samples/s/channel
Bits per second per Rx channel	19,200,000	bits/s/channel
Number of Rx channels	2	—
Total bits per second to storage device	38,400,000	bits/s
Total bytes per second to storage device	4,800,000	bytes/s

min: minimum; PRF: pulse repetition frequency; PRI: pulse repetition interval; RFI: RF interference.

2) *In-flight calibration*: A subset of premission measurements will be carried out periodically on every mission. Vernier adjustments will be made to meet mission requirements.
3) *Post flight/mission*: For each mission, a full before and after calibration and parameter scan provides the science data analytics group with the correct information needed for radargram processing.

ANTENNA SUBSYSTEM

Desert-SEA uses broadband correlation interferometry to estimate the off-nadir angle of surface returns in the cross-track direction. This will aid in discriminating the desired subsurface returns from undesired cross-track surface clutter.

Desert-SEA uses two separate mission-designed VHF, horizontally polarized, two-element folded-dipole array antennas that operate in the 45–95-MHz band to create subsurface images. To implement the interferometer capability, one antenna will be used as an Rx only and the other antenna will be switched between transmitting and receiving.

The antenna is one of the most critical Desert-SEA system elements. Analytical prototypes will be built and tested. The directivity of a single antenna (a two-element Yagi consisting of a folded dipole and a passive reflector) is expected to be a little higher than that of a dipole without a reflector, although the directivity is expected to vary over the broad operating band. The net gain per antenna (including RF loss) could be several decibels fewer than that of a resonant two-element Yagi due to the broadband matching network required for octave-band operation. The max directivity for interferometric operation would ideally be 3 dB higher than that of a single antenna. Including processing losses, interferometric processing should provide an SNR improvement of ~1.5 dB over single-antenna reception.

PROJECTED INSTRUMENT PERFORMANCE

The frequency and BW of the Desert-SEA's sounding radar are driven by the penetration depth requirements and the accuracy requirement for the water table depth measurement.

For a VHF sounding radar, four factors will affect the science return and influence the mission and instrument design.

PENETRATION DEPTH VARIABILITY

The science return from Desert-SEA is mainly driven by the ability of the radar wave to penetrate the subsurface, which is primarily governed by geoelectrical properties (i.e., dielectric properties and conductivity), and secondarily by the structural complexity of the explored ground. Geoelectrical properties define the dielectric attenuation in the radar signal, which is a function of soil composition, moisture content, and presence of clays and evaporites [28], [29], [63], [64], [65], [66], [67]. Hyperarid environments are widely known to be favorable geophysical environments for radar penetration (e.g., [42], [62], [68], [69], [70], and [71]). Scattering losses are small compared to the dielectric ones at the Desert-SEA's 45–95-MHz frequency [62], [72], [73]. The majority of the Sahara and the Arabian Peninsula is covered with erosional sediments that are mainly composed of desiccated, silica-rich materials that have low, one-way dielectric and scattering losses ranging from ~0.5 to 0.9 dB/m [28], [42], [62] [68], [71], [72], [74]. The latter yields average penetration depths of 50–100 m at 70 MHz under nominal conditions (i.e., lacking conductive minerals). Higher losses that can significantly constrain the penetration depth are located mainly near coastal areas and rivers [75]. These regions are not a part of Desert-SEA's science objectives.

RESOLVING SUBSURFACE FEATURES FROM CLUTTER

DESERT-SEA'S OVERALL SCIENCE GOAL IS TO CONSTRUCT DETAILED MAPS OF THE SPATIAL DISTRIBUTION OF SHALLOW AQUIFERS IN EARTH'S HYPERARID AREAS TO BETTER UNDERSTAND DESERT HYDROLOGY AND ENHANCE FLOW MODELS TO PROVIDE INSIGHTS INTO RECENT AND PAST CHANGES IN THESE AQUIFERS AND THEIR IMPLICATIONS FOR GROUNDWATER SUSTAINABILITY.

In hyperarid areas, shallow aquifers are located, by definition, in the flat, low-lying parts of basins, which are often filled with smooth sedimentary deposits, with h_{rms} less than 2 m within the radar's footprint [42]. Surface clutter, or echoes arising from surface features farther in the cross-track direction than the primary surface echo, can be confused with true subsurface returns, notably, ones from aquifers or their conduits, and therefore imposes a constraint on interpreting radar data from areas with significant surface topography (e.g., with hills adjacent to flat terrain) (see Figure 10). Moreover, to resolve the ambiguities arising from surface clutter, proven data processing methods that rely on digital elevation models (DEMs) and the geometry of radar propagation to predict the location of surface clutter in radargrams will be used [76], [77], [78], [79], [80]. Surface clutter, or echoes that arise from surface features farther in the cross-track direction than the primary surface echo, can be confused with true subsurface returns and therefore poses a constraint on interpreting radar data from areas with significant surface topography (e.g., hills adjacent to flat terrain) (Figure 10). By comparing clutter simulation results to the corresponding Desert-SEA radargrams, surface clutter can be distinguished from actual subsurface reflectors. DEMs with 90-m postings that are sufficient to calculate clutter for Desert-SEA are readily available for the targeted regions of interest; they are obtained from multiple missions, including the Advanced Spaceborne Thermal Emission and Reflection Radiometer (ASTER), Shuttle Radar Topography Mission (SRTM), and TanDEM-X. Resolving subsurface features from surface clutter was successfully

addressed for Earth and planetary sounding radars [28], [76], [77], [78], [81], [82], [83], [84], [85], [86].

OPTIMIZING THE RADAR'S BLIND ZONE

The blind zone of radar sounders is the region of the shallow subsurface washed out by very strong near-nadir surface returns. The blind zone gets deeper and brighter (increasingly cluttered with echoes from near-nadir surface reflections) as the altitude of the sensor increases due to a widening footprint. For a given depth, the depth-equivalent surface clutter point 1) moves farther away from nadir and 2) has steeper incident angles. These mean that 1) the isorange line of a target at depth at nadir overlaps with more volume and surface points and 2) any assumptions made about the surface scattering properties in analysis must be maintained over ever-increasing cross-track distances. For example, an airborne radar sounder at 1,000-m altitude that observes reflections from the water table interface located 20 m below a layer of desiccated, nonmagnetic, low-loss sand ($\varepsilon_r' = 3$) will observe overlapping reflections arriving at the same time (same range) from surface targets 30 m from nadir.

Depth resolution is inversely proportional to the transmitted waveform BW. Because the BW is limited, the depth resolution attainable in an airborne or spaceborne sounder is coarser than that achievable in a ground-level impulse GPR. The depth (range) resolution is given by $\rho_r = k_r c/(2Bn)$, where k_r is a range-resolution-broadening factor (whose value is approximately two) due to amplitude weighting for range sidelobe control, c is the speed of light, B is the waveform BW, and n is the refractive index in the subsurface medium. As the nadir surface return is strong, its mainlobe response can mask shallow subsurface returns within $\sim 0.75\rho_r$ from the surface (the aforementioned blind zone). For a 10-MHz waveform BW and a refractive index n of 1.73 (a conservative estimate of the relative permittivity in the subsurface medium of $\varepsilon_r' = 3$), this blind region extends to a depth of roughly 13 m. The blind region can

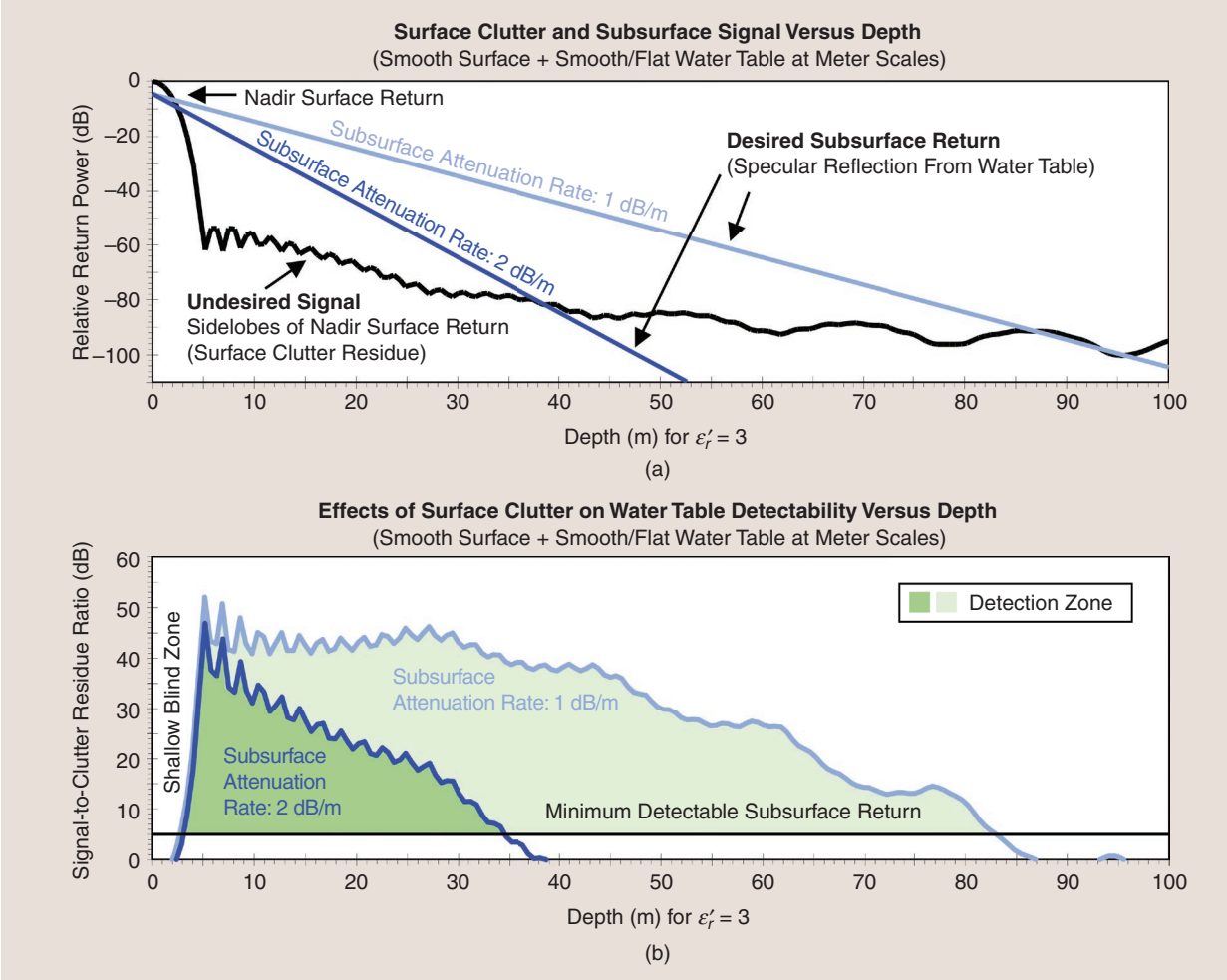

FIGURE 10. (a) The predicted nadir surface clutter response from a relatively smooth surface and the specular subsurface return power (from the water table) versus depth for $\varepsilon_r' = 3$ (dry sand) with two-way subsurface losses of 1 dB/m and 2 dB/m. (b) The difference (in decibels) of the curves in (a), i.e., the signal-to-clutter residue ratio of the subsurface water table reflections. The water table is detectable at depths where the subsurface return exceeds the surface clutter response. Adapted from Heggy et al. [42].

be reduced by increasing the waveform BW. For example, the blind region for systems with a 30-MHz BW waveform would be roughly 4.3 m deep, while that of a 50-MHz BW waveform would be approximately 2.6 m deep. In addition to minimizing the blind zone for deeper water table detection, the blind zone can also mask important information about dielectric variability in the shallowest 10–20 m of the subsurface, such as those from shallow, paleohydrological features, including remnant soil moisture.

Another significant factor affecting the extent of the blind zone for VHF sounders is surface roughness at the meter scale. The water table is, by definition, flat due to leveling of the fluid in the subsurface and does not follow the surface roughness. Hence, the desired subsurface returns are expected to be specular at the observation wavelength but must compete with the returns from surface clutter occurring at the same time delay. Near-specular nadir surface clutter returns (i.e., from a relatively smooth surface) are stronger than subsurface returns but are of limited time or range extent, enabling visibility of subsurface returns deeper than this blind zone, i.e., those occurring at later range delays. Clutter return signals (off-nadir surface returns) from a rough surface can be spread further in time, occupying ranges that can span the depths of interest.

If the surface clutter is near specular, as is the case for h_{rms} of 1 m in a 100 × 100-m footprint, it will mask subsurface returns only at shallow depths of ∼5 m. Hence, the water table is detectable at depths between 5 and 34 m for a conservative, two-way subsurface attenuation rate of 2 dB/m, as shown in Figure 10. However, for average two-way subsurface losses as small as 0.5 dB/m (e.g., [42]), the water table is detectable between depths of ∼5 and 83 m. Flying lower and decreasing the footprint size can improve the blind zone over areas with slightly higher h_{rms} (e.g., 2 m). We assume an h_{rms} below 1 or 2 m for Desert-SEA, which is achieved by operational altitudes of 500–2,000 m (yielding a surface footprint ≤20 m along track × 400 m across track) over the flat, smooth hydrological basins of interest [42]. Altogether, reliable observations of the subsurface returns therefore require some form of clutter mitigation that can be improved with altitude control and forward modeling of the clutter using existing DEMs of the surface.

EFFECTS OF EMI ON SURFACE SNR

Desert-SEA will operate over sparsely inhabited areas with few commercial radio or TV Txs. EMI from such sources (e.g., VHF-band television broadcasting towers) is a well-studied phenomenon in radar remote sensing. The successful mitigation of any EMI the Desert-SEA experiences imposes the following requirements: 1) that the radar operates with a wide dynamic range to avoid saturation and 2) that notch and/or adaptive filtering be applied during processing. To meet the first requirement, a ≥ 12-bit ADC will be used, with a ≥ 24-dB higher dynamic range than those previously used on orbital planetary radars [85].

Taken together, the aforementioned four factors strongly influence the requirements of the radar instrument's design, its operations, and its data processing.

SCIENCE ENHANCEMENT OPTIONS

The addition of three supporting off-the-shelf instruments provides an enhancement to the scientific return of the data acquired by the primary instrument, which is the sounding radar. These instruments are optical CCD/thermal cameras, a lidar, and a towed-bird FDEM induction sounder. The role and characteristics of each supporting instrument are briefly summarized as follows.

OPTICAL CCD/THERMAL CAMERAS

Three high-precision optical cameras (∼10-cm-per-pixel resolution at 1,000-m altitude), mounted forward, reverse, and downward looking, will enable the stacking of surface and subsurface images to provide a 3D cross-sectional view. These views can be used together with GPS data to accurately survey the probed surface and subsurface, land cover, and topography at the time of the survey. In addition, high-resolution images will be used to characterize surface conditions at the sounded sites (e.g., dunes, vegetation coverage, rough surfaces, and other features). Thermal CCDs can support the assessment of residual soil moisture.

THE INITIAL DEPLOYMENT OF THE DESERT-SEA AIRBORNE PROJECT WILL CONSIST OF ONLY THE RADAR SOUNDER, WHILE ENHANCED MISSION OPTIONS INCLUDE OFF-THE-SHELF OPTICAL CHARGE-COUPLED DEVICE AND THERMAL CAMERAS, LIDAR, AND A TOWED-BIRD FDEM.

LIDAR

The second auxiliary instrument is the lidar, which allows precise measurement of surface topography in several types of terrains, and is capable of measuring the intensity of the signal scattered by the surface, which depends on its optical (refractive index) and physical (roughness) properties. Lidar data will provide the 2 × 2-m topographic model necessary for accurately modeling and mitigating surface clutter in the radar-sounding data.

TOWED-BIRD FDEM

An airborne FDEM induction sounder towed in a pod ("bird") behind the aircraft ∼30 m above ground level can perform EM sounding for each site to determine the ground's vertical resistivity, a parameter crucial for understanding the salinity and radar response on site, as well as the interpretation of data in the postprocessing phase [87], [88]. Airborne FDEMs have a vertical resolution of a few meters to tens of meters, penetrate to depths of 100–150 m depending on soil resistivity, and are considerably more compact than time-domain EM systems, which require towing a large loop behind the aircraft (e.g., [58], [59], and [60]).

PROJECTED RESULTS AND DATA PLAN

Desert-SEA mission main data products will include a raw data archive (level 0 (L0) data); unprocessed position-registered time-domain radargrams (L1a); processed and calibrated position-registered depth-domain radargrams (L1b); processed, calibrated, and position-registered radargrams overlain with clutter simulations (L2); topography-corrected radargrams with identified water tables and topographic correction (L3); and 3D maps of the water table made from individual L3 profiles (L4).

L1 data will consist of pulse-compressed time-domain radar amplitude traces processed using signal summation to improve surface SNR. Clutter simulations for each track will be provided as part of the L1b data products. L2 data will consist of parameters extracted along each track, including surface topography and aquifer depth. Maps of shallow aquifer delineation and water table depth will be generated as well as examples of regional hydrogeological maps for the Nubian and Dammam aquifers (the largest fossil aquifers), which will be obtained by combining Desert-SEA's data with in situ geophysical datasets. The L0, L1 and L2 data product deliveries to the mission's data archive will begin within six months of downlink receipt and finish by the end of operations.

IMPLEMENTATION OPTIONS

The airborne VHF radar campaign is the main milestone of the Desert-SEA mission, where an aerial platform will be utilized to carry the new radar system and perform aquifer prospecting. Two implementation options are being considered: 1) helicopter based and 2) fixed-wing aircraft based.

(a)

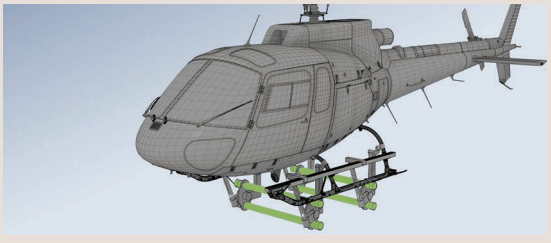

(b)

FIGURE 11. CAD renderings of the Desert-SEA radar antenna prototypes mounted on an AS350 helicopter. (a) A 200-MHz proof of concept (stowed configuration). (b) A full experiment with 70 MHz (deployed configuration).

HELICOPTER ROTORCRAFT

The baseline Desert-SEA radar flight vehicle will be the Aero Spatial 350 Utility Helicopter (Figure 11). The AS350 is readily available globally and supports the Desert-SEA's payload and power requirements and operation in areas spanning tens of kilometers. The sounder's flight kit consists of the following four major components:

1) *Antenna-mounting platform structure*: This provides a fixed platform for dual-directional VHF antennas and the integrated INS and GPS timing system. This modular system is designed for easy shipping, installation, and maintenance.
2) *Radar equipment support package*: This includes a Tx, an Rx, data processing, and storage components.
3) *Thermal design and management*: The nominal high-end operating temperature of Desert-SEA's sounding radar is 60 °C (140 °F). An integrated, systemwide thermal model of Desert-SEA's hardware package has been developed and will be used to guide subsystem component placement.
4) *Lightweight, quick-disconnect cable and harness system*: This is used for power, RF, digital, and flight safety systems.

The AS350 is widely used in radar-testing and surveying campaigns [89], [90] and has a successful heritage in airborne research experiments in various environments. It has the following performance characteristics:

- *Empty weight*: 1,174 kg (2,588 lb)
- *Max takeoff weight*: 2,250 kg (4,960 lb)
- *Engine power*: 632 kW (848 hp)
- *Cruise speed*: 245 km/h (152 mi/h, 132 kn)
- *Never-exceed speed*: 287 km/h (178 mi/h, 155 kn)
- *Range*: 662 km (411 mi, 357 nmi)
- *Endurance*: 4 h
- *Service ceiling*: 4,600 m (15,100 ft)
- *Rate of climb*: 8.5 m/s (1,670 ft/min).

The AS350 helicopter was successfully utilized for a lidar data campaign in Cambodia for deforestation observation. The flights were at altitudes of 800–1,000 m above ground level at a speed of 80 kn [89]. The AS350 was also utilized in NASA's Operation IceBridge [90], which intended to survey land and sea ice across the Arctic, Antarctic, and Alaska.

FIXED-WING AIRCRAFT

The alternative platform for Desert-SEA when considering coverage over larger areas (spanning a few hundred kilometers) is a fixed-wing aircraft that can be utilized to mount new radar systems and perform low-/high-altitude, long-range data acquisition campaigns. Fixed-wing aircrafts have the advantage of providing long-range flights in which vast amounts of data can be captured in one flight. Their longer range and altitude flexibility come with cost increases compared to the rotorcraft.

For the fixed-wing aircraft, the Dornier 228 model is considered for Desert-SEA flights. The Dornier 228 is a twin-engine, general-purpose aircraft capable of transporting up to 19 passengers or various cargo. It is powered by a pair of Garrett TPE331 turboprop engines. The Dornier 228 is commonly classified as a short takeoff and landing (STOL)-capable aircraft capable of operating from rough runways and in hot climates, which makes it suitable for Desert-SEA flights. This capability has been largely attributed to the type's supercritical wing, which generates large amounts of lift at slow speeds.

The Dornier 228 aircraft possesses the following specifications:

- *Empty weight*: 3,900 kg (8,598 lb)
- *Max takeoff weight*: 6,575 kg (14,495 lb)
- *Fuel capacity*: 1,885 kg
- *Powerplant*: 2 × TPE331-10 turboprop, 579 kW each
- *Cruise speed*: 413 km/h (257 mi/h, 223 kn)
- *Stall speed*: 137 km/h (85 mi/h, 74 kn)
- *Range*: 396 km (246 mi, 214 nmi), with a 1,960-kg payload
- *Ferry range*: 2,363 km (1,468 mi, 1,276 nmi), with a 547-kg payload
- *Endurance*: 10 h
- *Service ceiling*: 7,620 m (25,000 ft).

The Dornier 228 can provide more resources than rotorcrafts in terms of range, altitude, and speed for Desert-SEA flights. There are various possible installation locations of the radar prototype on the aircraft fuselage, one of which is on the bottom of the fuselage for nadir operation.

The Dornier 228 is typically promoted for its versatility, low operational costs, and high level of reliability. The Dornier 228 has been utilized for radar systems' testing experiments at various research institutions. The German Aerospace Center (DLR) has utilized two Dornier 228 aircraft to perform radar campaigns at both hot and arctic environment conditions [91]. The AfriSAR airborne SAR campaign in Gabon was executed to support development of the European Space Agency's Biomass P-band SAR satellite mission [91].

TARGETED STUDY SITES

High-resolution maps of the groundwater table can advance our understanding of the hydrogeology, paleohydrology, and paleoclimate in arid/hyperarid regions on Earth (e.g., the Saharan–Arabian Desert belt, Mojave Desert, Kalahari Desert, and Great Victoria Desert). Continuous data of groundwater table elevation, which will be obtained from Desert-SEA's radar sounding of shallow aquifers in the Arabian Peninsula, will certainly improve the present-day potentiometric maps that are interpolated from sparse-monitoring well data. These data, together with airborne topography data, will foster the development of integrated surface-groundwater flow modeling. Additionally, multitemporal flights over the same aquifer will provide a comprehensive understanding of the groundwater table fluctuation in response to groundwater abstraction and climate variability.

Here, we propose the preliminary candidate sites for conducting the airborne radar-sounding survey in the Arabian Peninsula (see Figure 12 and Table 4). The sites are distributed as follows:

- Two sites in Kuwait covering the Miocene–Pleistocene Kuwait Group aquifer in northern Kuwait (KW1) and the hydrologically connected Lower Kuwait unit and Dammam aquifer in southern Kuwait (KW2).
- Seven sites in Saudi Arabia covering the Cambrian Saq aquifer (SQ1, SQ2, SQ3, and SQ4), the Paleozoic Wajid aquifer (WJ1), and the Paleogene Umm er Radhuma aquifer (UER1 and UER2).
- A single site in eastern Oman covering the Tertiary-Quaternary Ash Sharqiyah Aquifer System (OM1).
- A single site in southern Qatar covering the Middle Eocene Dammam aquifer (QT1).
- A single site in the United Arab Emirates covering the Quaternary Sand Dunes (Liwa) aquifer (UAE1).

The selection of these sites considers:

- predefined aquifer areas with potential fresh or brackish water reserves and relevant aquifer materials (e.g., we did not consider fractured crystalline aquifer systems in Saudi Arabia and in Oman)
- shallow, unconfined, or semiconfined aquifer conditions (e.g., outcrop areas of deep aquifer systems and shallow, geologically recent aquifers)
- minimal soil-moisture conditions that minimize radar signal attenuation and maximize subsurface penetration (see Figure 10)
- low-conductive aquifer materials (i.e., areas were excluded where thick evaporites or other conductive material are encountered at shallow depths)
- validity for flight operation
- areas that will provide key insights into the regional aquifers' dynamics and connectivity.

PROOF OF CONCEPT AND FUTURE WORK

To identify high-risk subsystem areas that require specific attention in terms of design and potential adjustments to science requirements, we develop a 200-MHz "high-band" VHF sounder system as a proof of concept (POC) for the full-scale, high-power, VHF "low-band" (45–95-MHz) sounder. Implementing a POC system at 200 MHz reduces the risk in the antenna (e.g., design, fabrication, and installation) and allows the development effort to focus on other aspects of the system, including postflight signal processing algorithms and software. This phase will also refine cost and scheduling estimates of the mission concept.

In the following, we show how the 200-MHz POC is able to meet the key minimum requirements that achieve Desert-SEA's scientific objectives (see Table 1). The requirements for the 200-MHz POC radar sounder system are

- a minimum BW of 50 MHz or more (to achieve a vertical resolution of 3 m or better)

- a minimum 50-dB SNR or better at the surface (to achieve a max penetration depth of 20 m or more through arid desert sediments)
- a radiometric accuracy of 3 dB or better (to ascertain the physical characteristics of weakly backscattering subsurface reflectors at the aforementioned depths, including the top of the water table and stratigraphic features).

The 200-MHz POC radar sounder provides empirical evidence that the aforementioned minimum requirements are technically achievable in terms of concepts, hardware, algorithms, and calibration plans, and that the operational

FIGURE 12. A distribution of the proposed flight zones in the Arabian Peninsula. SQ: Cambrian Saq aquifer; WJ: Paleozoic Wajid aquifer; UER: Umm er Radhuma aquifer; KW: Kuwait; QT: Qatar; OM: Oman.

TABLE 4. AQUIFER CHARACTERISTICS OF THE PROPOSED FLIGHT ZONES.

AQUIFER	COUNTRY	AGE	ZONE	ZONE AREA (KM^2)
Kuwait Group aquifer	Kuwait (KW)	Mio-Pleistocene	KW1	4,550
Kuwait Group and Dammam aquifers	Kuwait	Eocene to Pleistocene	KW2	4,964
Saq aquifer (SQ)	Saudi Arabia	Cambrian	SQ4	12,027
Saq aquifer	Saudi Arabia	Cambrian	SQ2	12,220
Saq aquifer	Saudi Arabia	Cambrian	SQ3	7,575
Saq aquifer	Saudi Arabia	Cambrian	SQ1	8,855
Wajid (WJ) aquifer	Saudi Arabia	Paleozoic	WJ1	35,921
Umm er Radhuma (UER) aquifer	Saudi Arabia	Paleogene	UER1	5,467
Umm er Radhuma aquifer	Saudi Arabia	Paleogene	UER2	2,041
Ash Sharqiyah Aquifer System	Oman (OM)	Tertiary-Quaternary	OM1	2,300
Dammam aquifer	Qatar (QT)	Eocene	QT1	4,472
Quaternary Sand Dunes (Liwa) aquifer	United Arab Emirates (UAE)	Quaternary	UAE1	17,444

TABLE 5. THE POC SUMMARY.

CHALLENGE	SOLUTION
Use of software-defined radio (SDR) technology	• Employed direct conversion (homodyne) multichannel SDR approach to provide necessary sensitivity and dynamic range • Allows quick adaptation to varying RF emission requirements and national/local spectrum regulations • Conducted low-level, end-to-end testing of Desert-SEA Tx/Rx chain.
Operating high-power, high-repetition, near-ground radar systems	• Tailored Tx/Rx chain, focusing on waveform design and implementing automatic gain control for a high instantaneous dynamic range • Mitigates Rx overload, prevents Tx/Rx switches products from saturating the ADC, and reduces blind zone.
Modeling and development of suitable antenna	*High-band antenna*: • Identified off-the-shelf folded-dipole array antenna operating at 200 MHz that meets size, weight, and radiation pattern requirements • Provides the necessary BW with a 0–2-dB gain, and suitable for deployment on fixed and rotary-wing aircraft. *Low-band VHF antenna (70 MHz)*: • Identified off-the-shelf 50-MHz BW folded-dipole array.
Mitigation of Tx waveform sidelobes	• Modeled and bench tested various techniques including waveform windowing, chirp pulse compression, Tx and matched digital Rx filtering, and system calibration algorithms • Aimed to improve target detection and enhance clutter rejection • Analyzed clutter rejection requirements and initial Tx power spectrum.
Efficient high-power pulse VHF signal PA	• Modeled, designed, and tested modular approach to generate required 500-W Tx waveform • Provides necessary prelaunch power, enabling a minimum of 200-W EIRP • Ensures future upgradability for low-band radar use for Desert-SEA.

EIRP: effective isotropic radiated power.

procedures planned for the low-band Desert-SEA radar will work as intended. The POC also allows for various ground and airborne evaluation scenarios to reveal and resolve functionality, durability, and reliability issues.

The key POC sounder hardware and software characteristics are driven by the science requirements, as shown in Table 1). Specifically,

- *surface SNR*, which is an indirect metric of max penetration depth, is achieved through high Tx power (500 W), high antenna efficiency, and minimization of system losses.
- *radiometric accuracy* is attained by accurate antenna pattern characterization, accurate measurement of the Tx output power, and measurement of the system noise using a calibrated noise source. Optionally, in-flight calibration could be done by collecting data over a smooth water surface if one is available.
- *vertical resolution* and *blind-zone depth* requirements are met through the proper selection of the waveform BW and pulse-compression weighting functions. A subsurface vertical resolution requirement of 3 m drives the waveform BW to approximately 50 MHz.

The primary challenges addressed thus far during the POC phase are summarized in Table 5. One of these is the antenna system design and its electrical and mechanical implementation on the aircraft. To overcome this challenge, our design utilizes compact, high-efficiency, wideband folded-dipole structures that can be securely mounted and resist vibrational and environmental damage.

Another challenge addressed in the POC is efficient high-power operation, which requires an airborne-compliant, lightweight, wideband pulse amplifier design operating with a moderate-to-high PRF ranging from 5 to 15 kHz and pulsewidths from 1 to 5 µs. Recent advances in commercial semiconductor development make this requirement feasible.

Moreover, to minimize interference with national, international, and commercial wireless systems, out-of-band RF signal components must be highly suppressed per national government requirements. This requires highly linear RF subsystems to minimize harmonic distortion and spectral regrowth components, i.e., that the Desert-SEA Tx's out-of-band energy is attenuated to a noninterfering level, and in-band products are minimized to preserve coherency and Rx signal feature visibility. Herein, we demonstrate the capability of the PA exciter to successfully address these constraints for the 200-MHz sounder in Figures 13–15.

Signal processing for the Desert-SEA high-band POC uses a high-speed programmable FPGA to generate both the required Tx wave for the suite, along with precision system test and calibration waveforms. Rx signal processing consists of sampling and storing high-definition samples of the transmitted and received signal for coherent postflight processing into human- and machine-interpretable radargrams. Prior to storage, received raw data streams are processed to maximize SNR in an expected high-clutter and interference environment.

In the future, during planned flight tests with the Desert-SEA 200-MHz sounder, deep machine learning deep neural network (DNN) techniques will be applied to the quick-look interpretation of the collected radargrams for visualization during acquisition. The data volume generated for a single flight zone during airborne operations (referring to Figure 12 and Table 4) is expected to be on the order of a few terabytes. This DNN process simplifies and improves the overall accuracy, efficacy, and speed of identifying potentially water-saturated zones and groundwater conduits in the subsurface in real time for further detailed postacquisition radargram processing.

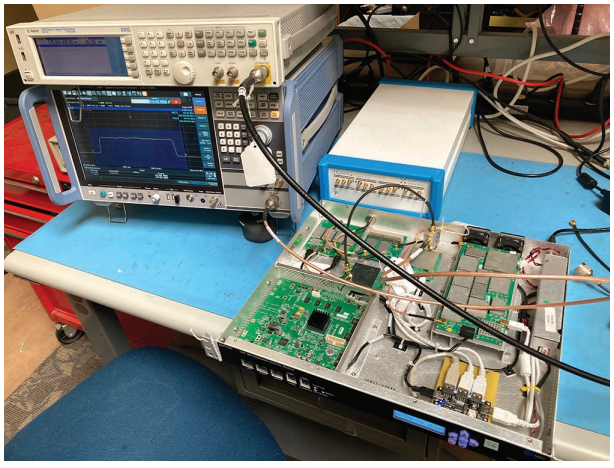

FIGURE 13. Testing of the Desert-SEA Tx chain PA driver in the 170–230-MHz band before integration into the bench model.

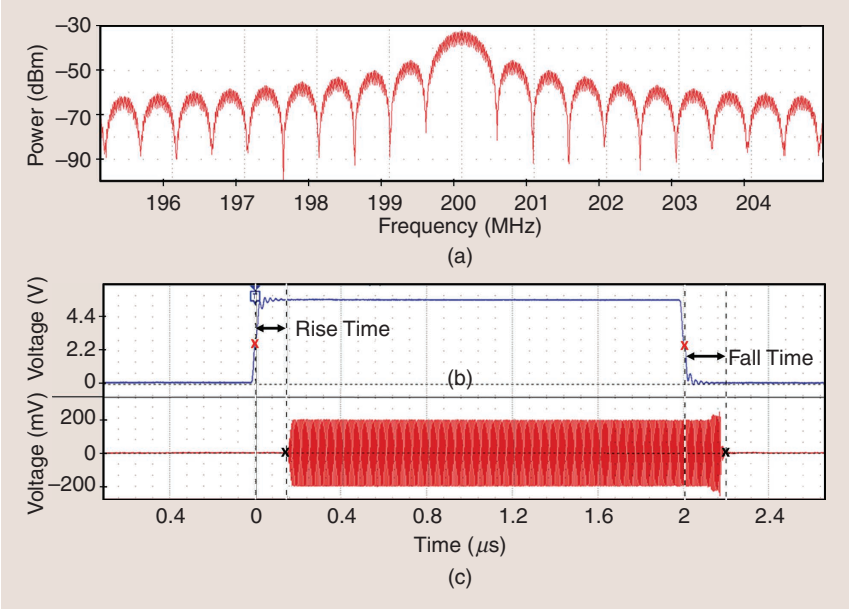

FIGURE 14. The frequency- and time-domain responses of the Desert-SEA PA driver (2-μs pulse at –30 dBm or 1 μW) demonstrating the relatively fast rise and fall times and the symmetrical spectral response centered on 200 MHz. (a) Power spectrum of Tx waveform. (b) T/R switch gating pulse. (c) Outgoing RF pulse.

Training the DNN model will involve integrating various data sets, such as existing remote sensing data, flight data, meteorological data, geospatial data, DEMs, and land-use images. Mission planning, including site selection, flight planning, premission, ground and airborne equipment checkout, calibration protocols, data collection mission scheme, postmission data processing and analysis, and reporting of mission results, will also be critical.

In summary, we have shown that Desert-SEA's minimum requirements are readily achievable with current off-the-shelf subsystem components. As radar subsystem technologies continue to develop, we will therefore be able to exceed these minimum requirements. For example, advances in software-defined radios that decrease noise and increase sampling improve the overall SNR, which is the key challenge for such systems.

CONCLUSIONS AND OUTLOOK

Herein, we provided the concept for an airborne, wideband VHF sounding radar operating at a central frequency of 70 MHz that will perform large-scale mapping and characterization of the water table of shallow aquifers in hyperarid environments at meter-scale resolution: Desert-SEA. We defined the concept's science and instrument requirements, designed the system that meets these requirements, and tested its subsystems to demonstrate feasibility. Through discrete, multiday airborne sounding radar campaigns, surveying areas of the Sahara and Arabian deserts where shallow aquifers are being recharged or discharging—i.e., probing the shallow subsurface while tracing grids with lines extending tens of kilometers long and separated by a few hundred meters—Desert-SEA is expected to provide crucial knowledge in these key locations that constrain the uncertainty on the dynamics of larger aquifer systems that remain poorly understood. Expanding the coverage of these campaigns in the upcoming decades will ultimately yield high-resolution maps of the depths and extents of the water table in most of today's shallow aquifers in these hyperarid areas, surpassing the existing maps derived from sparse, unevenly distributed well logs. By achieving these objectives, Desert-SEA can significantly improve our current understanding of how these large water bodies respond to climatic and anthropogenic stressors. This gained knowledge will provide a more sustainable water management strategy for these globally

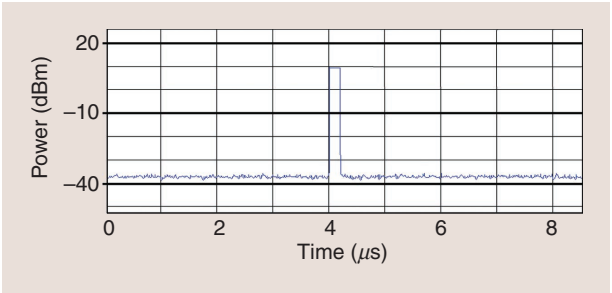

FIGURE 15. A Tx output power profile demonstrating the ability to produce a shorter pulsewidth (100 ns at 10 dBm or 10 mW), which is required for the operational goal of flying at lower altitudes to enhance surface SNR.

depleting aquifers and provide crucial insights to better model their future response to increasing water demand and hydroclimatic fluctuations in arid areas [92], [93].

The aforementioned requirements can be met using the VHF sounding radar described herein, which consists of two linearly polarized folded-dipole array antennas—enabling a BW of 50 MHz—and a surface SNR of 85 dB (postprocessing) that surveys from an altitude ranging from 500 to 2,000 m, depending on the surface topography and roughness. We show that these requirements can be met using the radar design and subsystems presented herein, primarily utilizing off-the-shelf components with moderate customized programming of the digital part of the radar. Hence, the feasibility of such a system is high and cost-effective, enabling the replication of such an experiment in several areas where large-scale subsurface mapping is needed. The system's expected performance is its ability to map the uppermost water table depths of aquifer systems that span tens of kilometers, at a vertical resolution of 3 m in desiccated terrains to an average penetration depth of 50 m, and with a spatial resolution of 200 m. These expected water table depth maps exceed the resolution of existing ones by one or two orders of magnitude, allowing a more accurate understanding and modeling of groundwater dynamics in hyperarid areas.

The continuation of the POC phase in future work will bring Desert-SEA from a technology readiness level (TRL) of four to six (comprising flight tests and testing the 200-MHz POC sounder in the United States, including the Sleeping Bear Dunes in Michigan or other dune fields), after which the full flight model will be developed to bring it from a TRL of seven to nine.

The data produced from Desert-SEA's survey campaigns will be archived and made publicly available with multiple product levels (L1–L4), providing new knowledge to assess and model shallow aquifer dynamics and groundwater resources in hyperarid deserts.

ACKNOWLEDGMENT

The authors are very grateful to John Wilson of the United States Agency for International Development (USAID), and Paul Rosen, Anthony Freeman, Ken Wolfenbarger, Ziad Haddad, and Charles Elachi of the Jet Propulsion Laboratory and California Institute of Technology (Caltech) for their support, which initiated this work. The authors are also grateful to Nabil Alhusseini of the Bin Omran Trading & Telecommunications Company for his generous donation to the University of Southern California (USC) Arid Climates and Water Research (AWARE) Center, which enabled a large part of this research development.

This work was supported in part by the USAID under the Further Advancing the Blue Revolution Initiative (FABRI) under Grant 1001624-13S-19790 attributed to Caltech and USC for PI Essam Heggy; in part by the Keck Space Institute at Caltech for PI Jean-Philippe Avouac and PI Essam Heggy; in part by the Zumberge Research and Innovation Fund of USC allocated to the AWARE Center; and in part by a research agreement between USC and the Qatar Environment and Energy Research Institute at Hamad Bin Khalifa University in Qatar. The work of Tamer Khattab was funded by QR-DI-QNRF grant no. AICC03-0530-200033. The work of Elizabeth M. Palmer and of Sayed M. Bateni was supported by the U.S. Department of State Bureau of Educational and Cultural Affairs under Fulbright U.S. Scholar Awards 11563-QA and 10563-QA, respectively. Essam Heggy is the corresponding author.

AUTHOR INFORMATION

Essam Heggy (heggy@usc.edu) is with the Department of Electrical and Computer Engineering, University of Southern California, Los Angeles, CA 90089 USA, and also with the NASA Jet Propulsion Laboratory, California Institute of Technology, Pasadena, CA 91109 USA, and the Qatar Environment and Energy Research Institute, Hamad Bin Khalifa University, Doha, Qatar. He is a Member of IEEE.

Mahta Moghaddam (mahta@usc.edu) is with the Department of Electrical and Computer Engineering, University of Southern California, Los Angeles, CA 90089 USA. She is a Fellow of IEEE.

Elizabeth M. Palmer (elizabeth.m.palmer@usc.edu) is with the Department of Electrical and Computer Engineering, University of Southern California, Los Angeles, CA 90089 USA. She is a Member of IEEE.

William M. Brown (bbrown121944@gmail.com) is with Metric Systems Corporation, Carlsbad, CA 92011 USA. He is a Member of IEEE.

J. Lee Blanton (j.l.blanton@ieee.org) is with Metric Systems Corporation, Carlsbad, CA 92011 USA. He is a Member of IEEE.

Mikołaj Kosinski (mikoaj.kosinski@gmail.com) is with the Department of Electrical and Computer Engineering, University of Southern California, Los Angeles, CA 90089 USA.

Paul Sirri (paulsirri@gmail.com) is with the Department of Electrical and Computer Engineering, University of Southern California, Los Angeles, CA 90089 USA.

Edgar A. Dixon (de5@usf.edu) is with the Department of Electrical and Computer Engineering, University of Southern California, Los Angeles, CA 90089 USA.

Abotalib Z. Abotalib (afarag@usc.edu) is with the Division of Geological Applications and Mineral Resources, National Authority for Remote Sensing and Space Sciences, Cairo, Egypt, and also with the Department of Electrical and Computer Engineering, University of Southern California, Los Angeles, CA 90089 USA.

Jonathan C. L. Normand (normand@usc.edu) is with the Department of Electrical and Computer Engineering, University of Southern California, Los Angeles, CA 90089 USA. He is a Member of IEEE.

John Clark (jeclark2006@aim.com) is with Metric Systems Corporation, Carlsbad, CA 92011 USA.

Gary Klemens (gklem19165@gmail.com) is with Metric Systems Corporation, Carlsbad, CA 92011 USA.

Matthieu Agranier (matthieu.agranier@polytechnique.edu) is with the Department of Electrical and Computer Engineering, University of Southern California, Los Angeles, CA 90089 USA.

François Guillon (francois.guillon@polytechnique.edu) is with the Department of Electrical and Computer Engineering, University of Southern California, Los Angeles, CA 90089 USA.

Akram A. Abdellatif (akram.abdellatif@tum.de) is with the Institute of Flight System Dynamics, Technical University of Munich, 80333 Munich, Germany.

Tamer Khattab (tkhattab@ieee.org) is with the Department of Electrical Engineering, Qatar University, Doha, Qatar. He is a Senior Member of IEEE.

Zlatan Tsvetanov (ztsvetanov@hbku.edu.qa) is with the Qatar Environment and Energy Research Institute, Hamad Bin Khalifa University, Doha, Qatar.

Mohamed Shokry (shokry@binomran.com) is with the Bin Omran Trading & Telecommunications WLL, Doha, Qatar.

Noor Al-Mulla (nma91@georgetown.edu) is with the Department of Electrical and Computer Engineering, University of Southern California, Los Angeles, CA 90089 USA.

Mohamed Ramah (m.ramah94@gmail.com) is with the Earth and Life Institute, Catholic University of Louvain, B-1348 Louvain-la-Neuve, Belgium.

Sayed M. Bateni (smbateni@hawaii.edu) is with the Department of Civil and Environmental Engineering, University of Hawai'i at Mānoa, Honolulu, HI 96822 USA.

Alireza Tabatabaeenejad (alireza.tabatabaeenejad@aero.org) is with The Aerospace Corporation, El Segundo, CA 90245 USA. He is a Senior Member of IEEE.

Jean-Philippe Avouac (avouac@caltech.edu) is with the Division of Geological and Planetary Sciences, California Institute of Technology, Pasadena, CA 91125 USA. He is a Member of IEEE.

REFERENCES

[1] "The United Nations world water development report 2022: Groundwater: Making the invisible visible," United Nations, New York, NY, USA, 2022. [Online]. Available: https://www.unwater.org/publications/un-world-water-development-report-2022

[2] W. Wagner, *Groundwater in the Arab Middle East*. Berlin, Germany: Springer-Verlag, 2011.

[3] H. Tabari, "Climate change impact on flood and extreme precipitation increases with water availability," *Scientific Rep.*, vol. 10, no. 1, pp. 1–10, Aug. 2020, doi: 10.1038/s41598-020-70816-2.

[4] O. El-Saadawy, A. Gaber, A. Othman, A. Z. Abotalib, M. El Bastawesy, and M. Attwa, "Modeling flash floods and induced recharge into alluvial aquifers using multi-temporal remote sensing and electrical resistivity imaging," *Sustainability*, vol. 12, no. 23, Dec. 2020, Art. no. 10204, doi: 10.3390/su122310204.

[5] M. M. Khalil, T. Tokunaga, E. Heggy, and A. Z. Abotalib, "Groundwater mixing in shallow aquifers stressed by land cover/land use changes under hyper-arid conditions," *J. Hydrol.*, vol. 598, Jul. 2021, Art. no. 126245, doi: 10.1016/j.jhydrol.2021.126245.

[6] W. Aeschbach-Hertig and T. Gleeson, "Regional strategies for the accelerating global problem of groundwater depletion," *Nature Geosci.*, vol. 5, no. 12, pp. 853–861, 2012, doi: 10.1038/ngeo1617.

[7] A. Z. Abotalib, E. Heggy, G. Scabbia, and A. Mazzoni, "Groundwater dynamics in fossil fractured carbonate aquifers in Eastern Arabian Peninsula: A preliminary investigation," *J. Hydrol.*, vol. 571, pp. 460–470, Apr. 2019, doi: 10.1016/j.jhydrol.2019.02.013.

[8] M. O. Cuthbert, et al., "Global patterns and dynamics of climate–groundwater interactions," *Nature Climate Change*, vol. 9, no. 2, pp. 137–141, 2019, doi: 10.1038/s41558-018-0386-4.

[9] K. Abdelmohsen, M. Sultan, H. Save, A. Z. Abotalib, and E. Yan, "What can the GRACE seasonal cycle tell us about lake-aquifer interactions?" *Earth Sci. Rev.*, vol. 211, Dec. 2020 Art. no. 103392, doi: 10.1016/j.earscirev.2020.103392.

[10] S. S. Fouad et al., "Egypt's waterways conservation campaigns under growing intrinsic demand and Nile upstream damming," *J. Hydrol., Regional Stud.*, vol. 50, Dec. 2023, Art. no. 101537, doi: 10.1016/j.ejrh.2023.101537.

[11] R. G. Taylor et al., "Ground water and climate change," *Nature Climate Change*, vol. 3, no. 4, pp. 322–329, Apr. 2013, doi: 10.1038/nclimate1744.

[12] A. Z. Abotalib, E. Heggy, M. El Bastawesy, E. Ismail, A. Gad, and M. Attwa, "Groundwater mounding: A diagnostic feature for mapping aquifer connectivity in hyper-arid deserts," *Sci. Total Environ.*, vol. 801, Dec. 2021, Art. no. 149760, doi: 10.1016/j.scitotenv.2021.149760.

[13] K. Abdelmohsen, M. Sultan, H. Save, A. Z. Abotalib, E. Yan, and K. H. Zahran, "Buffering the impacts of extreme climate variability in the highly engineered Tigris Euphrates river system," *Scientific Rep.*, vol. 12, no. 1, Mar. 2022, Art. no. 4178, doi: 10.1038/s41598-022-07891-0.

[14] A. C. Amanambu et al., "Groundwater system and climate change: Present status and future considerations," *J. Hydrol.*, vol. 589, Oct. 2020, Art. no. 125163, doi: 10.1016/j.jhydrol.2020.125163.

[15] E. Heggy, P. A. Rosen, R. Beatty, T. Freeman, and Y. Gim, "Orbiting Arid Subsurface and Ice Sheet Sounder (OASIS): Exploring desert aquifers and polar ice sheets and their role in current and

paleo-climate evolution," in *Proc. IEEE Int. Geosci. Remote Sens. Symp. (IGARSS)*, Melbourne, Australia, Jul. 2013, pp. 3483–3486, doi: 10.1109/IGARSS.2013.6723579.

[16] A. Mazzoni, E. Heggy, and G. Scabbia, "Forecasting water budget deficits and groundwater depletion in the main fossil aquifer systems in North Africa and the Arabian Peninsula," *Global Environ. Change*, vol. 53, pp. 157–173, Nov. 2018, doi: 10.1016/j.gloenvcha.2018.09.009.

[17] E. Heggy, Z. Sharkawy, and A. Z. Abotalib, "Egypt's water budget deficit and suggested mitigation policies for the Grand Ethiopian Renaissance Dam filling scenarios," *Environ. Res. Lett.*, vol. 16, no. 7, Jul. 2021, Art. no. 074022, doi: 10.1088/1748-9326/ac0ac9.

[18] S. S. Fouad, E. Heggy, A. Z. Abotalib, M. Ramah, S. Jomaa, and U. Weilacher, "Landscape-based regeneration of the Nile Delta's waterways in support of water conservation and environmental protection," *Ecological Indicators*, vol. 145, Dec. 2022, Art. no. 109660, doi: 10.1016/j.ecolind.2022.109660.

[19] M. C. Peel, B. L. Finlayson, and T. A. McMahon, "Updated world map of the Köppen-Geiger climate classification," *Hydrol. Earth Syst. Sci.*, vol. 11, no. 5, pp. 1633–1644, Oct. 2007, doi: 10.5194/hess-11-1633-2007.

[20] W. Terink, W. W. Immerzeel, and P. Droogers, "Climate change projections of precipitation and reference evapotranspiration for the Middle East and Northern Africa until 2050," *Int. J. Climatol.*, vol. 33, no. 14, pp. 3055–3072, Nov. 2013, doi: 10.1002/joc.3650.

[21] A. M. MacDonald et al., "Mapping groundwater recharge in Africa from ground observations and implications for water security," *Environ. Res. Lett.*, vol. 16, no. 3, Mar. 2021, Art. no. 034012, doi: 10.1088/1748-9326/abd661.

[22] A. Z. Abotalib, M. Sultan, and R. Elkadiri, "Groundwater processes in Saharan Africa: Implications for landscape evolution in arid environments," *Earth Sci. Rev.*, vol. 156, pp. 108–136, May 2016, doi: 10.1016/j.earscirev.2016.03.004.

[23] "Transboundary aquifers of the world," International Groundwater Resources Assessment Centre, Delft, The Netherlands, 2021. [Online]. Available: https://www.un-igrac.org/ggis/transboundary-aquifers-world-map

[24] N. C. Sturchio et al., "One million year old groundwater in the Sahara revealed by krypton-81 and chlorine-36," *Geophys. Res. Lett.*, vol. 31, no. 5, Mar. 2004, Art. no. 2003GL019234, doi: 10.1029/2003GL019234.

[25] B. Khezzani and S. Bouchemal, "Variations in groundwater levels and quality due to agricultural over-exploitation in an arid environment: The phreatic aquifer of the Souf oasis (Algerian Sahara)," *Environ Earth Sci.*, vol. 77, no. 4, Feb. 2018, Art. no. 142, doi: 10.1007/s12665-018-7329-2.

[26] M. Yousif, H. M. Hussien, and A. Z. Abotalib, "The respective roles of modern and paleo recharge to alluvium aquifers in continental rift basins: A case study from El Qaa plain, Sinai, Egypt," *Sci. Total Environ.*, vol. 739, Oct. 2020, Art. no. 139927, doi: 10.1016/j.scitotenv.2020.139927.

[27] M. Sultan et al., "Natural discharge: A key to sustainable utilization of fossil groundwater," *J. Hydrol.*, vol. 335, nos. 1–2, pp. 25–36, Mar. 2007, doi: 10.1016/j.jhydrol.2006.10.034.

[28] E. Heggy et al., "On water detection in the Martian subsurface using sounding radar," *Icarus*, vol. 154, no. 2, pp. 244–257, Dec. 2001, doi: 10.1006/icar.2001.6717.

[29] D. Mukherjee, E. Heggy, and S. D. Khan, "Geoelectrical constraints on radar probing of shallow water-saturated zones within karstified carbonates in semi-arid environments," *J. Appl. Geophys.*, vol. 70, no. 3, pp. 181–191, Mar. 2010, doi: 10.1016/j.jappgeo.2009.11.005.

[30] A. Milewski et al., "A remote sensing solution for estimating runoff and recharge in arid environments," *J. Hydrol.*, vol. 373, nos. 1–2, pp. 1–14, Jun. 2009, doi: 10.1016/j.jhydrol.2009.04.002.

[31] J.-C. Fontes, M. Yousfi, and G. B. Allison, "Estimation of long-term, diffuse groundwater discharge in the northern Sahara using stable isotope profiles in soil water," *J. Hydrol.*, vol. 86, nos. 3–4, pp. 315–327, Oct. 1986, doi: 10.1016/0022-1694(86)90170-8.

[32] M. Sultan et al., "Geochemical, isotopic, and remote sensing constraints on the origin and evolution of the Rub Al Khali aquifer system, Arabian Peninsula," *J. Hydrol.*, vol. 356, nos. 1–2, pp. 70–83, Jul. 2008, doi: 10.1016/j.jhydrol.2008.04.001.

[33] A. Nada, T. M. Abd-El Maksoud, M. Abu-Zeid Hosnia, T. El-Nagar, and S. Awad, "Distribution of radionuclides in soil samples from a petrified wood forest in El-Qattamia, Cairo, Egypt," *Appl. Radiat. Isot.*, vol. 67, no. 4, pp. 643–649, Apr. 2009, doi: 10.1016/j.apradiso.2008.11.016.

[34] A. Z. Abotalib and R. S. A. Mohamed, "Surface evidences supporting a probable new concept for the river systems evolution in Egypt: A remote sensing overview," *Environ. Earth Sci.*, vol. 69, no. 5, pp. 1621–1635, Jul. 2013, doi: 10.1007/s12665-012-1998-z.

[35] P. Hoelzmann, D. Jolly, S. P. Harrison, F. Laarif, R. Bonnefille, and H.-J. Pachur, "Mid-Holocene land-surface conditions in northern Africa and the Arabian Peninsula: A data set for the analysis of biogeophysical feedbacks in the climate system," *Global Biogeochem. Cycles*, vol. 12, no. 1, pp. 35–51, Mar. 1998, doi: 10.1029/97GB02733.

[36] J. McCauley et al., "Paleodrainages of the Eastern Sahara—the radar rivers revisited (SIR-A/B implications for a mid-Tertiary Trans-African drainage system)," *IEEE Trans. Geosci. Remote Sensing*, vol. GE-24, no. 4, pp. 624–648, Jul. 1986, doi: 10.1109/TGRS.1986.289678.

[37] P. Paillou et al., "Mapping of a major paleodrainage system in eastern Libya using orbital imaging radar: The Kufrah River," *Earth Planet. Sci. Lett.*, vol. 277, nos. 3–4, pp. 327–333, Jan. 2009, doi: 10.1016/j.epsl.2008.10.029.

[38] C. Skonieczny et al., "African humid periods triggered the reactivation of a large river system in Western Sahara," *Nat. Commun.*, vol. 6, no. 1, Nov. 2015, Art. no. 8751, doi: 10.1038/ncomms9751.

[39] H. S. Groucutt and M. D. Petraglia, "The prehistory of the Arabian peninsula: Deserts, dispersals, and demography," *Evol. Anthropol.*, vol. 21, no. 3, pp. 113–125, May/Jun. 2012, doi: 10.1002/evan.21308.

[40] W. E. Galloway and J. M. Sharp, "Hydrogeology and characterization of fluvial aquifer systems," in *Hydrogeologic Models of Sedimentary Aquifers*, G. S. Fraser and J. M. Davis, Eds., Tuksa, OK, USA: SEPM Society for Sedimentary Geology, 1998, pp. 91–106.

[41] M. El Bastawesy, E. Gebremichael, M. Sultan, M. Attwa, and H. Sahour, "Tracing Holocene channels and landforms of the Nile Delta through integration of early elevation, geophysical, and sediment core data," *Holocene*, vol. 30, no. 8, pp. 1129–1141, Aug. 2020, doi: 10.1177/0959683620913928.

[42] E. Heggy et al., "Probing shallow aquifers in hyperarid dune fields using VHF sounding radar," *IEEE Trans. Geosci. Remote Sens.*, vol. 61, pp. 1–22, Aug. 2023, doi: 10.1109/TGRS.2023.3306286.

[43] L. C. Davis, "Electrostatic edge modes of a dielectric wedge," *Phys. Rev. B*, vol. 14, no. 12, pp. 5523–5525, Dec. 1976, doi: 10.1103/PhysRevB.14.5523.

[44] S. Lambot, E. Slob, D. Chavarro, M. Lubczynski, and H. Vereecken, "Measuring soil surface water content in irrigated areas of southern Tunisia using full-waveform inversion of proximal GPR data," *Near Surface Geophys.*, vol. 6, no. 6, pp. 403–410, Dec. 2008, doi: 10.3997/1873-0604.2008028.

[45] S. F. Shih, J. A. Doolittle, D. L. Myhre, and G. W. Schellentrager, "Using radar for groundwater investigation," *J. Irrigation Drain Eng.*, vol. 112, no. 2, pp. 110–118, May 1986, doi: 10.1061/(ASCE)0733-9437(1986)112:2(110).

[46] G. C. Bohling, M. P. Anderson, and C. R. Bentley, "Use of ground penetrating radar to define recharge areas in the Central Sand Plain," NASA STI/Recon, Washington, DC, USA, Tech. Rep., Jan. 1989. [Online]. Available: https://ui.adsabs.harvard.edu/abs/1989STIN...9012814B/abstract

[47] Y. Lévesque, R. Chesnaux, and J. Walter, "Using geophysical data to assess groundwater levels and the accuracy of a regional numerical flow model," *Hydrogeol. J.*, vol. 31, no. 2, pp. 351–370, 2023, doi: 10.1007/s10040-023-02591-z.

[48] E. Heggy, A. Fadlelmawla, T. G. Farr, and M. Al-Rashed, "Probing shallow aquifers in Northern Kuwait using airborne sounding radars," *presented at the Amer. Geophys. Union Fall Meeting*, San Francisco, CA, USA, Dec. 2011, No. P13G-06, ADS Bibcode: 2011AGUFM.P13G.06H.

[49] G. G. Schaber, J. F. McCauley, and C. S. Breed, "The use of multifrequency and polarimetric SIR-C/X-SAR data in geologic studies of Bir Safsaf, Egypt," *Remote Sens. Environ.*, vol. 59, no. 2, pp. 337–363, Feb. 1997, doi: 10.1016/S0034-4257(96)00143-5.

[50] P. Paillou, G. Grandjean, N. Baghdadi, E. Heggy, T. August-Bernex, and J. Achache, "Subsurface imaging in south-central Egypt using low-frequency radar: Bir Safsaf revisited," *IEEE Trans. Geosci. Remote Sens.*, vol. 41, no. 7, pp. 1672–1684, Jul. 2003, doi: 10.1109/TGRS.2003.813275.

[51] P. Paillou, S. Lopez, T. Farr, and A. Rosenqvist, "Mapping subsurface geology in Sahara using L-Band SAR: First results from the ALOS/PALSAR imaging radar," *IEEE J. Sel. Topics Appl. Earth Observ. Remote Sens.*, vol. 3, no. 4, pp. 632–636, Dec. 2010, doi: 10.1109/JSTARS.2010.2056915.

[52] P. Paillou, S. Lopez, E. Marais, and K. Scipal, "Mapping paleohydrology of the ephemeral Kuiseb River, Namibia, from radar remote sensing," *Water*, vol. 12, no. 5, May 2020, Art. no. 1441, doi: 10.3390/w12051441.

[53] C. I. Voss and S. M. Soliman, "The transboundary non-renewable Nubian Aquifer System of Chad, Egypt, Libya and Sudan: Classical groundwater questions and parsimonious hydrogeologic analysis and modeling," *Hydrogeol. J.*, vol. 22, no. 2, pp. 441–468, 2014, doi: 10.1007/s10040-013-1039-3.

[54] K. E. N. Howard and A. Griffith, "Can the impacts of climate change on groundwater resources be studied without the use of transient models?" *Hydrol. Sci. J.*, vol. 54, no. 4, pp. 754–764, 2009, doi: 10.1623/hysj.54.4.754.

[55] Z. W. Kundzewicz et al., "Freshwater resources and their management," in *Climate Change 2007: Impacts, Adaptation and Vulnerability. Contribution of Working Group II to the Fourth Assessment Report of the Intergovernmental Panel on Climate Change*, M. L. Parry, O. F. Canziani, J. P. Palutikof, P. J. van der Linden, and C. E. Hanson, Eds., Cambridge, U.K.: Cambridge Univ. Press, 2007, pp. 173–210. [Online]. Available: www.ipcc.ch/site/assets/uploads/2018/03/ar4_wg2_full_report.pdf

[56] N. S. Diffenbaugh, D. L. Swain, D. Touma, and J. Lubchenco, "Anthropogenic warming has increased drought risk in California," *Proc. Nat. Acad. Sci. U.S.A*, vol. 112, no. 13, pp. 3931–3936, 2015, doi: 10.1073/pnas.1422385112.

[57] S. Stevenson et al., "Twenty-first century hydroclimate: A continually changing baseline, with more frequent extremes," *Proc. Nat. Acad. Sci. U.S.A*, vol. 119, no. 12, 2022, Art. no. e2108124119, doi: 10.1073/pnas.2108124119.

[58] B. Siemon, "Electromagnetic methods – Frequency domain: Airborne techniques," in *Groundwater Geophysics: A Tool for Hydrogeology*, R. Kirsch, Ed., Berlin, Germany: Springer Science & Business Media, 2006, pp. 155–170.

[59] A. Viezzoli, "Airborne electromagnetics for groundwater salinity mapping: Case studies of coastal and inland salinization from around the world," *Bollettino di Geofisica Teorica ed Applicata*, vol. 53, no. 4, pp. 581–600, 2012, doi: 10.4430/bgta0067.

[60] M. Karaoulis, I. Ritsema, C. Bremmer, and M. De Kleine, "Drone-borne electromagnetic (DREM) surveying in The Netherlands," in *Proc. 26th Eur. Meeting Environ. Eng. Geophys. (NSG)*, 2020, pp. 1–5, doi: 10.3997/2214-4609.202020032.

[61] V. Zlotnicki and D. Stammer, "Applying spaceborne gravity measurements to ocean studies," *Eos Trans. AGU*, vol. 92, no. 17, pp. 145–145, Apr. 2011, doi: 10.1029/2011EO170007.

[62] E. Heggy, S. M. Clifford, R. E. Grimm, C. L. Dinwiddie, D. Y. Wyrick, and B. E. Hill, "Ground-penetrating radar sounding in mafic lava flows: Assessing attenuation and scattering losses in Mars-analog volcanic terrains," *J. Geophys. Res.*, vol. 111, no. E6, 2006, Art. no. E06S04, doi: 10.1029/2005JE002589.

[63] G. R. Olhoeft, "Low-frequency electrical properties," *Geophysics*, vol. 50, no. 12, pp. 2492–2503, Dec. 1985, doi: 10.1190/1.1441880.

[64] E. Heggy et al., "Local geoelectrical models of the Martian subsurface for shallow groundwater detection using sounding radars," *J. Geophys. Res. Planet*, vol. 108, no. E4, 2003, Art. no. 8030, doi: 10.1029/2002JE001871.

[65] J. Boisson et al., "Sounding the subsurface of Athabasca Valles using MARSIS radar data: Exploring the volcanic and fluvial hypotheses for the origin of the rafted plate terrain," *J. Geophys. Res. Planets*, vol. 114, no. E8, pp. 1–12, Aug. 2009, doi: 10.1029/2008JE003299.

[66] J. Boisson, E. Heggy, S. M. Clifford, K. Yoshikawa, A. Anglade, and P. Lognonné, "Radar sounding of temperate permafrost in Alaska: Analogy to the Martian midlatitude to high-latitude

ice-rich terrains," *J. Geophys. Res. Planets*, vol. 116, no. E11, Nov. 2011, Art. no. E11003, doi: 10.1029/2010JE003768.

[67] Y. Berquin, A. Herique, W. Kofman, and E. Heggy, "Computing low-frequency radar surface echoes for planetary radar using Huygens-Fresnel's principle," *Radio Sci*, vol. 50, no. 10, pp. 1097–1109, 2015, doi: 10.1002/2015RS005714.

[68] P. Hoekstra and A. Delaney, "Dielectric properties of soils at UHF and microwave frequencies," *J. Geophys. Res.*, vol. 79, no. 11, pp. 1699–1708, Apr. 1974, doi: 10.1029/JB079i011p01699.

[69] T. Farr, C. Elachi, P. Hartl, and K. Chowdhury, "Microwave penetration and attenuation in desert soil: A field experiment with the shuttle imaging radar," *IEEE Trans. Geosci. Remote Sens.*, vol. GE-24, no. 4, pp. 590–594, Jul. 1986, doi: 10.1109/TGRS.1986.289675.

[70] C. Elachi, K. E. Im, F. Li, and E. Rodriguez, "Global digital topography mapping with a synthetic aperture scanning radar altimeter," *Int. J. Remote Sens.*, vol. 11, no. 4, pp. 585–601, Apr. 1990, doi: 10.1080/01431169008955043.

[71] P. Paillou et al., "Performances of ground penetrating radars in arid volcanic regions: Consequences for Mars subsurface exploration," *Geophys. Res. Lett.*, vol. 28, no. 5, pp. 911–914, 2001, doi: 10.1029/1999GL008449.

[72] E. Heggy, S. M. Clifford, R. E. Grimm, C. L. Dinwiddie, J. A. Stamatakos, and S. H. Gonzalez, "Low-frequency radar sounding investigations of the North Amargosa Desert, Nevada: A potential analog of conductive subsurface environments on Mars," *J. Geophys. Res. Planets*, vol. 111, no. E6, Art. no. E06S03, 2006, doi: 10.1029/2005JE002523.

[73] R. E. Grimm, E. Heggy, S. Clifford, C. Dinwiddie, R. McGinnis, and D. Farrell, "Absorption and scattering in ground-penetrating radar: Analysis of the Bishop Tuff," *J. Geophys. Res.*, vol. 111, no. E6, 2006, Art. no. E06S02, doi: 10.1029/2005JE002619.

[74] F. T. Ulaby, R. K. Moore, and A. K. Fung, *Microwave Remote Sensing. 2: Radar Remote Sensing and Surface Scattering and Emission Theory*. Reading, MA, USA: Addison-Wesley, 1982.

[75] G. Koh, "Radar attenuation in desert soil," presented at the SPIE Defense Secur. Symp., Orlando, FL, USA, Apr. 2008, Art. no. 69530X, doi: 10.1117/12.777816.

[76] G. Picardi et al., "Radar soundings of the subsurface of Mars," *Science*, vol. 310, no. 5756, pp. 1925–1928, Dec. 2005, doi: 10.1126/science.1122165.

[77] J. W. Holt, M. E. Peters, S. D. Kempf, D. L. Morse, and D. D. Blankenship, "Echo source discrimination in single-pass airborne radar sounding data from the Dry Valleys, Antarctica: Implications for orbital sounding of Mars," *J. Geophys. Res.*, vol. 111, no. E6, 2006, Art. no. E06S24, doi: 10.1029/2005JE002525.

[78] J. W. Holt et al., "Radar sounding evidence for buried glaciers in the southern mid-latitudes of Mars," *Science*, vol. 322, no. 5905, pp. 1235–1238, Nov. 2008, doi: 10.1126/science.1164246.

[79] M. G. Spagnuolo, F. Grings, P. Perna, M. Franco, H. Karszenbaum, and V. A. Ramos, "Multilayer simulations for accurate geological interpretations of SHARAD radargrams," *Planet. Space Sci.*, vol. 59, nos. 11–12, pp. 1222–1230, 2011, doi: 10.1016/j.pss.2010.10.013.

[80] B. A. Campbell and T. R. Watters, "Phase compensation of MARSIS subsurface sounding data and estimation of ionospheric properties: New insights from SHARAD results," *J. Geophys. Res. Planet*, vol. 121, no. 2, pp. 180–193, 2016, doi: 10.1002/2015JE004917.

[81] A. Safaeinili, W. Kofman, J.-F. Nouvel, A. Herique, and R. L. Jordan, "Impact of Mars ionosphere on orbital radar sounder operation and data processing," *Planet. Space Sci.*, vol. 51, nos. 7–8, pp. 505–515, Jun. 2003, doi: 10.1016/S0032-0633(03)00048-5.

[82] A. Safaeinili et al., "Estimation of the total electron content of the Martian ionosphere using radar sounder surface echoes," *Geophys. Res. Lett.*, vol. 34, no. 23, pp. 1–6, Dec. 2007, Art. no. L23204, doi: 10.1029/2007GL032154.

[83] R. J. Phillips et al., "Mars north polar deposits: Stratigraphy, age, and geodynamical response," *Science*, vol. 320, no. 5880, pp. 1182–1185, May 2008, doi: 10.1126/science.1157546.

[84] J. Mouginot, W. Kofman, A. Safaeinili, and A. Herique, "Correction of the ionospheric distortion on the MARSIS surface sounding echoes," *Planetary Space Sci.*, vol. 56, no. 7, pp. 917–926, May 2008, doi: 10.1016/j.pss.2008.01.010.

[85] R. Jordan et al., "The Mars express MARSIS sounder instrument," *Planetary Space Sci.*, vol. 57, nos. 14–15, pp. 1975–1986, Dec. 2009, doi: 10.1016/j.pss.2009.09.016.

[86] B. A. Campbell, D. M. Schroeder, and J. L. Whitten, "Mars radar clutter and surface roughness characteristics from MARSIS data," *Icarus*, vol. 299, pp. 22–30, Jan. 2018, doi: 10.1016/j.icarus.2017.07.011.

[87] B. Siemon, A. V. Christiansen, and E. Auken, "A review of helicopter-borne electromagnetic methods for groundwater exploration," *Near Surface Geophys.*, vol. 7, no. 5–6, pp. 629–646, Oct. 2009, doi: 10.3997/1873-0604.2009043.

[88] S. Costabel, B. Siemon, G. Houben, and T. Günther, "Geophysical investigation of a freshwater lens on the island of Langeoog, Germany – Insights from combined HEM, TEM and MRS data," *J. Appl. Geophys.*, vol. 136, pp. 231–245, Jan. 2017, doi: 10.1016/j.jappgeo.2016.11.007.

[89] M. Singh et al., "Evaluating remote sensing datasets and machine learning algorithms for mapping plantations and successional forests in Phnom Kulen National Park of Cambodia," *PeerJ*, vol. 7, Oct. 2019, Art. no. e7841, doi: 10.7717/peerj.7841.

[90] J. A. MacGregor et al., "The scientific legacy of NASA's Operation IceBridge," *Rev. Geophys.*, vol. 59, no. 2, Jun. 2021, Art. no. e2020RG000712, doi: 10.1029/2020RG000712.

[91] R. Horn et al., "F-SAR-recent upgrades and campaign activities," in *Proc. 18th Int. Radar Symp. (IRS)*, Jun. 2017, pp. 1–10, doi: 10.23919/IRS.2017.8008092.

[92] E. Heggy, M. Ramah, and A. Z. Abotalib, "Examining the accuracy of using a single short-term historical flow period to assess the Nile's downstream water deficit from GERD filling: A technical note," *Earth Syst. Environ.*, vol. 7, no. 4, pp. 723–732, Dec. 2023, doi: 10.1007/s41748-023-00355-z.

[93] R. Noori et al., "Decline in Iran's groundwater recharge," *Nature Commun.*, vol. 14, no. 1, Oct. 2023, Art. no. 6674, doi: 10.1038/s41467-023-42411-2.

GRS